NSTX

Stress Analysis of Inner PF Coils (1a, 1b & 1c), Center Stack Upgrade

NSTXU-CALC-133-01-01

April 09, 2012

Prepared By:

_____

Leonard Myatt, Myatt Consulting, Inc. (BOA 04613-F)

Reviewed By:

_____

Art Brooks, Engineering Analyst

_____

Ali Zolfaghari, Engineering Analyst

Reviewed By:

_____

James H. Chrzanowski, NSTX Cognizant Engineer

PPPL Calculation Form

Calculation #   **NSTXU-CALC-133-01-01**   Revision # **01**__   WP #, **1672** (ENG-033)

Purpose of Calculation: (Define why the calculation is being performed.)

To qualify the structural capacity of the Inner PF coils (1a, 1b & 1c) for use in the NSTX upgrade (See 2.0 Introduction)

References:

See 6.0 References.

Assumptions: (Identify all assumptions made as part of this calculation.)

1. Vacuum pressure impregnated (VPI) coils behave as bonded monoliths and do not experience significant conductor-epoxy bond degradation which would change their structural characteristics.
2. Structural elements are joined by full-penetration welds except where explicitly modeled as fillets.
3. Bolted flanges are sufficiently preloaded to preclude opening/separation during coil operation.
4. Plasma currents are modeled as a constant current density over the idealized "shaped" or "circular" cross-sections.
5. Cool-down from the potting cure temperature produces stresses which are benign (single-cycle, secondary) compared with the operating loads.

Calculation: (Calculation is either documented here or attached.)

See 4.0 Analysis

Note:
The section 4.6 of this calculation was prepared by Ali Zolfaghari and reviewed by Leonard Myatt. The sections1.0 through 4.3.13.2 were checked by Art Brooks and sections 4.4, 4.5 & 4.7 were checked by Ali Zolfaghari.

Conclusion: (Specify whether or not the purpose of the calculation was accomplished.)

This analysis of the inner PF coils has aided in the design evolution to a point where they satisfy the project's structural design criteria for all 480 proposed plasma and post plasma-disruption equilibria. However, coil power supplies are capable of driving currents which would likely produce coil failures. Consequently, a Digital Coil Protection (DCP) algorithm must be designed and implemented to ensure safe PF coil operation.

Cognizant Engineer's printed name, signature, and date

James Chrzanowski _____

I have reviewed this calculation and, to my professional satisfaction, it is properly performed and correct.

Checker's printed name, signature, and date

Art Brooks _____

Ali Zolfaghari _____

Table of Contents

1.0 Executive Summary

A structural assessment of the NSTX Center Stack Upgrade (CSU) Inner PF coils (PF1a/1b/1c) is presented based on finite element simulations of the coils and their supports. Simulation begins with a parametric 2D ANSYS EM model used to calculate Lorentz forces for 96 equilibria and five different plasma conditions, as defined in Neumeyer's Design Point Spreadsheet ([1] DPS). These ANSYS result also serve as a benchmark for the force calculations in the spreadsheet which shows spot-checked agreement to <1%. Of these 480 EM operating points, only a few are found to be structurally limiting based on various screening algorithms. These significant operating points have their EM forces imported into an axisymmetric representation of the coil and structure. In regions where the geometry is non-axisymmetric, various 3D models are developed and used to evaluate such details.

Stresses in the conductor, insulation and support structure are reviewed and evaluated relative to the project's structural design criteria NSTX_CRIT-0001-01a ([2] SDC). Where appropriate, design changes are recommended, incorporated and re-evaluated in order to ultimately achieve a sufficiently robust coil and structure system. For example:

- Epoxy/glass insulation shear stress levels require the beneficial effects of priming the conductor in order to achieve an optimal copper-to-epoxy bond.
- The lower support is changed from a few discrete legs to a gusseted cylindrical shell structure
- Outer bands are added to the 1a (1/8" thick) and 1b (3/16" thick) open mandrel coils in order to stiffen these structures and provide a centering mechanism. However, the height over which the coil and band interact must be limited.
- The 1c coil case needs to be modified to be conceptually similar to the mandrel plus outer band structure used for 1a and 1b. In this case, the band can be only 1/8" thick and, again, the height over which the coil and band interact must be limited.
- Lead support configuration designed to isolate bus bar loads while providing enough flexibility to accommodate radial motion from warm, end of pulse winding pack growth.

Analysis shows that these inner PF coils can be operated over the 480 EM operating point electromagnetic and thermal design space. However, there is the potential for coils to operate at currents within their power supply limits which would result in significant loads on the structure. Consequently, a Digital Coil Protection (DCP) algorithm must be developed and used to limit coil currents and max temperature to ensure safe operation.

Thanks to Lew Morris for evolving the design and providing numerous solid model images.

2.0 Introduction

While the Center Stack upgrade includes many changes, the work presented here focuses on the inner PF coils (Upper & Lower 1a, 1b & 1c) and their associated support structure. Evaluating coils and their structures always involves calculating electromagnetic (Lorentz) body forces. Coil dimensions (Rc, Zc, dr, dz, nr, nz, dr_con, dz_con, d_hole, t_tw, t_gw) are required inputs and C. Neumeyer has thoughtfully formatted these (tab "PF_Coil_Parameters_ANSYS_Input") to match the ANSYS input file requirements. Coil currents are also defined in the spreadsheet, although much more involve since there are 96 plasma equilibria, each with five different plasma conditions:

- ➢ No plasma
- ➢ 2MA Circular plasma
- ➢ 2MA Shaped plasma
- ➢ Following the disruption of a 2MA Circular plasma
- ➢ Following the disruption of a 2MA Shaped plasma

The structure is defined by a series of CAD models provided by L. Morris as SAT files. These CAD models are simplified to some degree, which makes them easier to "mesh" and subsequently reduces the computational requirements resulting in reasonable analysis run-times.

Scoping studies make use of an efficient, axisymmetric structural model with smeared wind pack (WP) properties, in which hundreds of equilibria are evaluated based on coil and support structure stress levels. Another screening technique is employed to find a few of the most critical operating conditions which produce the largest radial or vertical load on coils and groups of coils. As a result of these scoping studies, only a hand full of operating currents emerge as worthy of refined analysis with detailed 2D WP models or 3D structures.
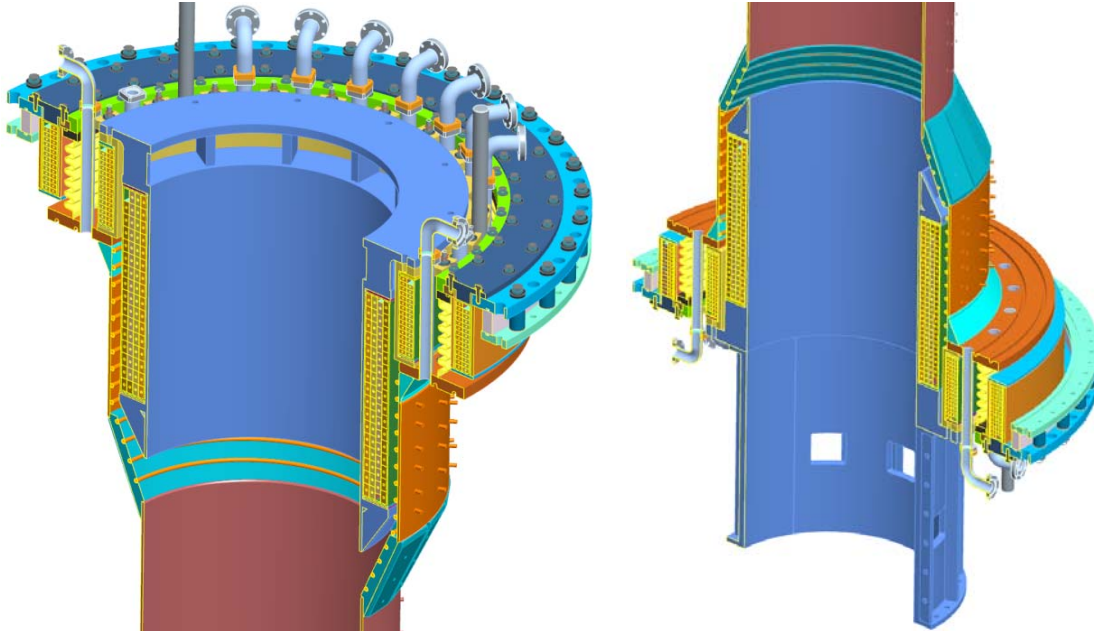

Fig. 2.0-1 Close-Ups of Upper and Lower Inner PF coils, including Gusseted Shell Support

3.0 Assumptions

1. Vacuum pressure impregnated (VPI) coils behave as bonded monoliths and do not experience significant conductor-epoxy bond degradation which would change their structural characteristics.
2. Structural elements are joined by full-penetration welds except where explicitly modeled as fillets.
3. Bolted flanges are sufficiently preloaded to preclude opening/separation during coil operation.
4. Plasma currents are modeled as a constant current density over the idealized "shaped" or "circular" cross-sections.
5. Cool-down from the potting cure temperature produces stresses which are benign (single-cycle, secondary) compared with the operating loads.

4.0 Analysis

A parametric, 2D ANSYS EM model of the PF coil system is developed as shown in Fig. 4.0-1. Coil currents can either be applied to discrete conductors (not discernible on this scale) or smeared winding packs. An input parameter allow for defining the plasma cross-section as either *shaped* (geometric parameters listed in title) or *circular* ($\Delta=0$, $K=1$).

The design space is extensive: (96) equilibria operating points for (5) different plasma conditions. EM fields and forces are calculated for each of the 96 equilibria current sets and five plasma conditions. Net coil forces are spot checked with other project force calculations. Sample field results are shown in Fig. 4.0-2 where the inner PF coils are modeled as discrete conductors and the plasma is *shaped*.

The EM model is turned into an axisymmetric approximation of the PF1 coils and their accompanying support structure, as shown in Fig. 4.0-3.

- ➢ Detailed WPs (including turn and ground insulation) are imported from EM model.
- ➢ Contact elements between the WP and the support structured (all six PF1 coils).
- ➢ The lower support is added.
- ➢ Upper and lower PF1c coils are supported by a displacement boundary condition (BC) to simulate the support of the vacuum vessel (VV).
- ➢ Loads are imported from the EM results (ANSYS *LDREAD* command).

Although the coils are nominally axisymmetric, some elements of the supporting structures are 3D. A 360° model of the PF1a and 1b upper structure and a sector model of PF1c are developed as shown in Fig. 4.0-4. Worse-case EM and thermal loads are applied and stresses from these 2D and 3D models are evaluated.
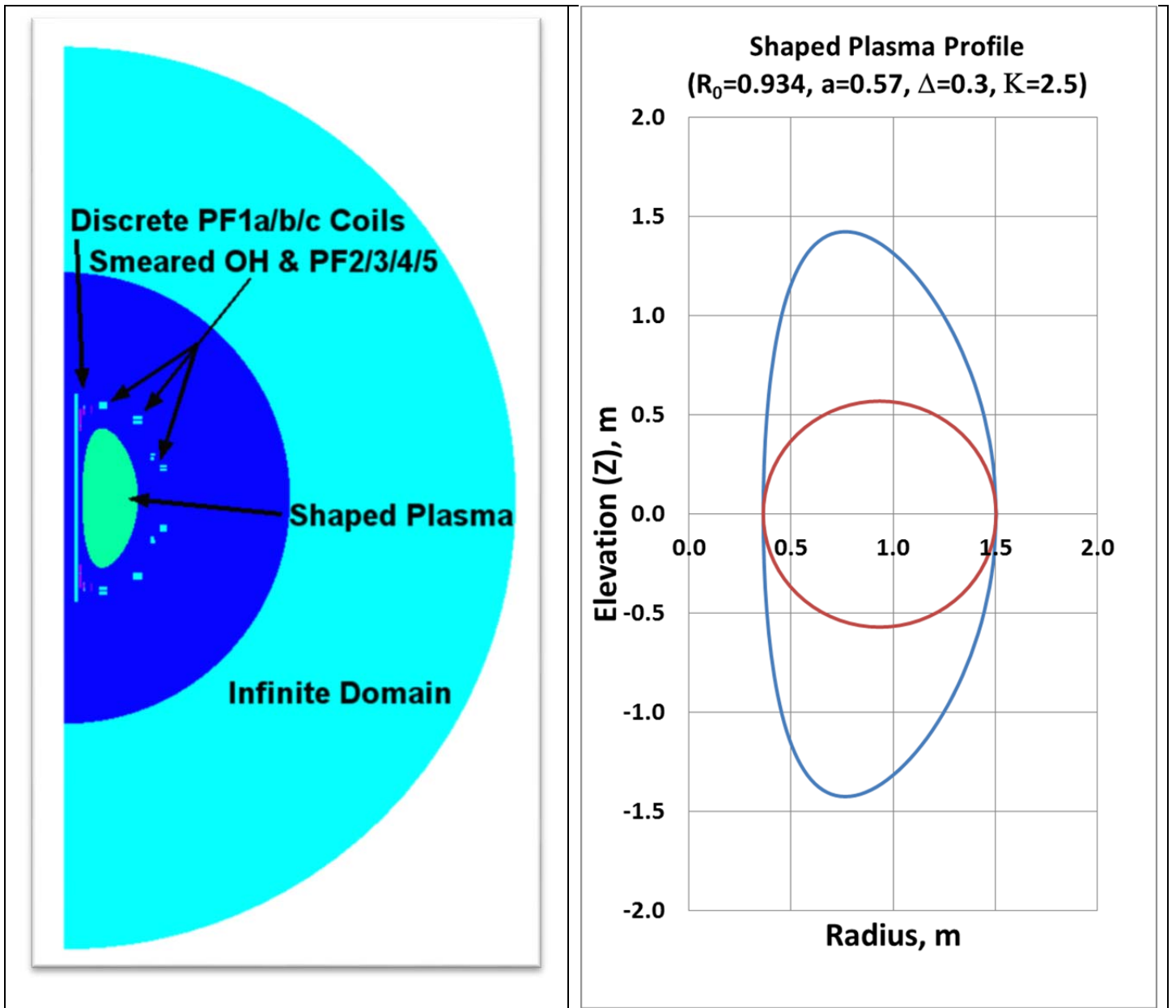
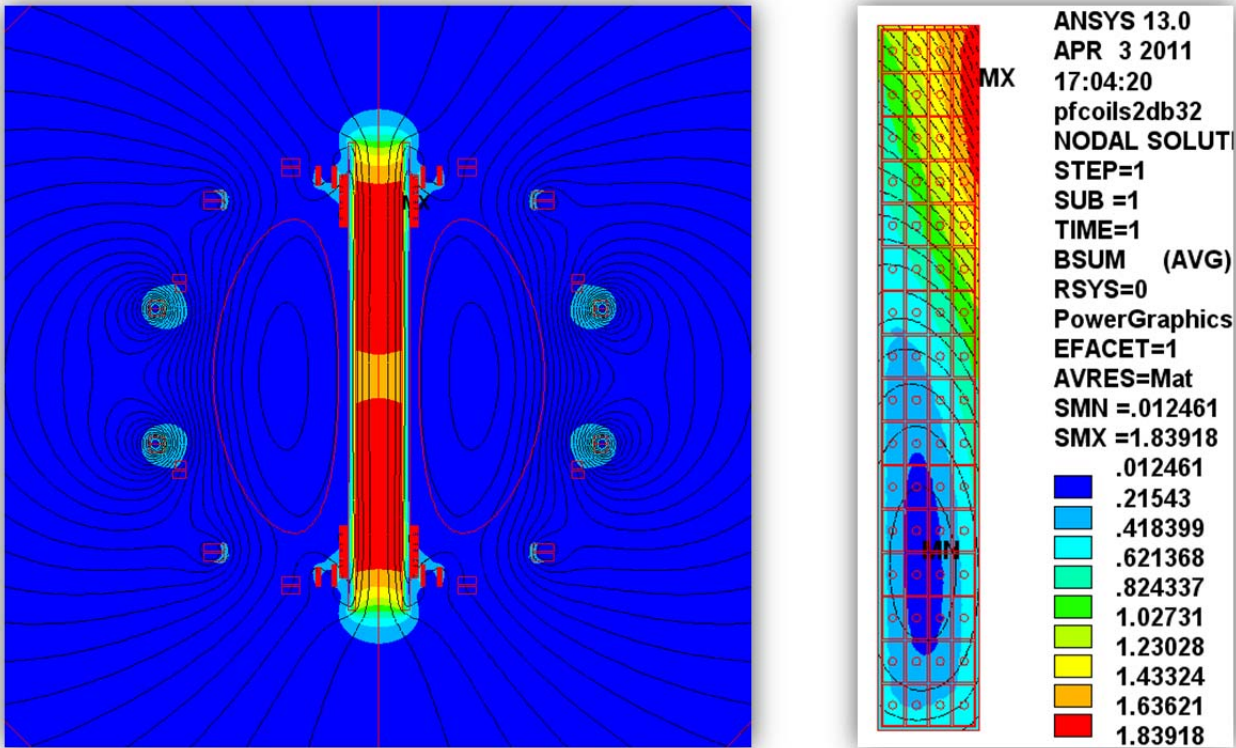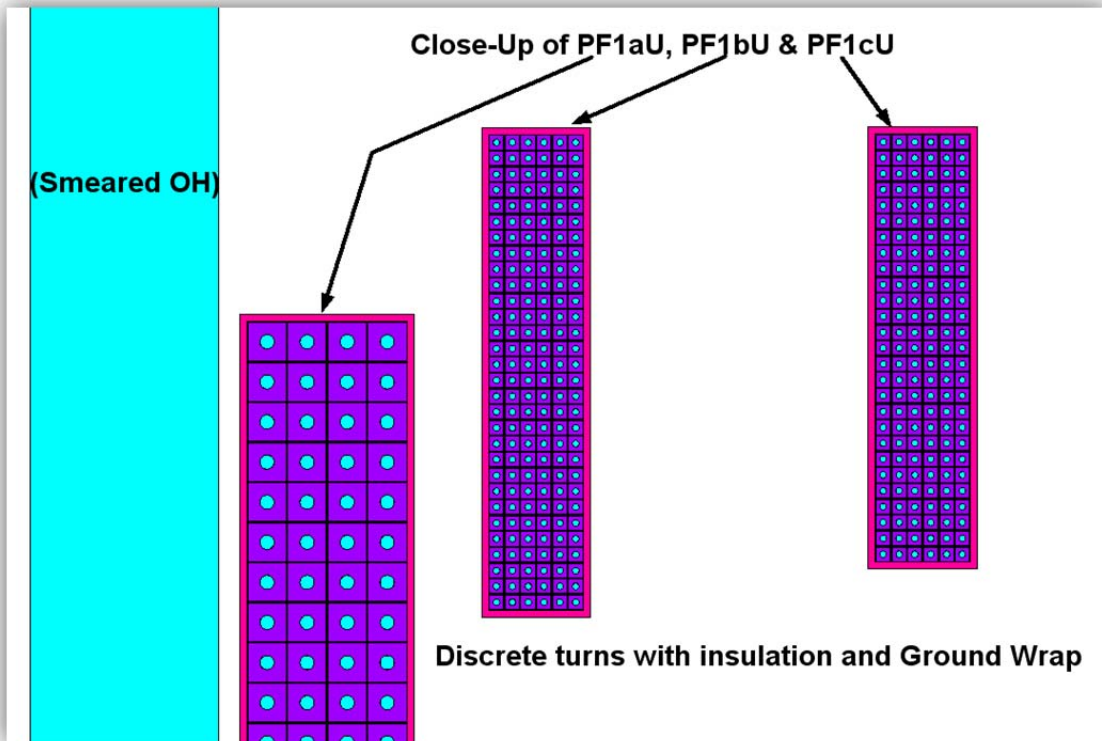Fig. 4.0-1 Axisymmetric Field Model of NSTX Poloidal Field Sources (OH, PF and Plasma)

Fig. 4.0-2 Sample Results: Flux Density with AZ, Flux Density in Discretely Modeled PF1a
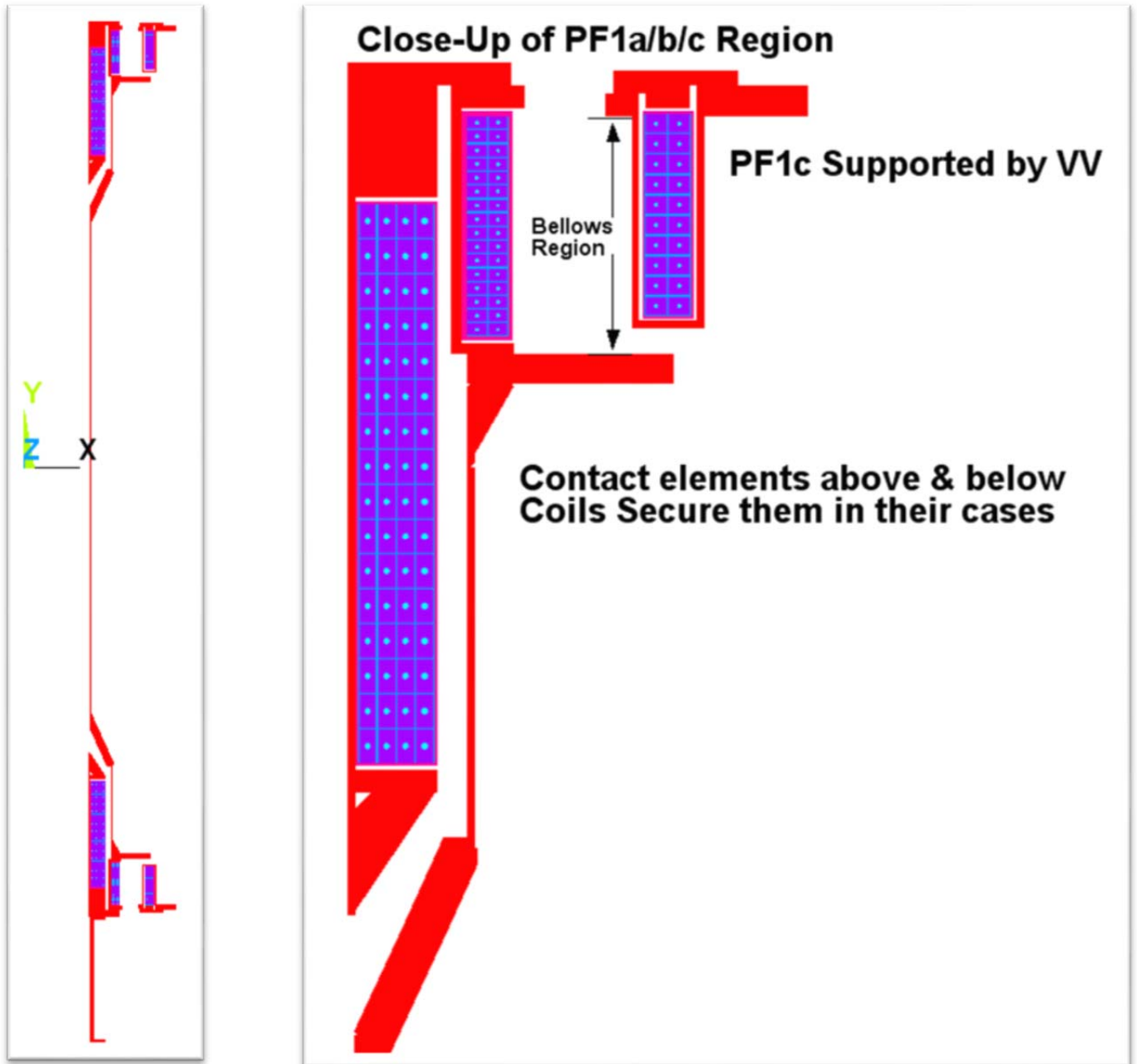
Fig. 4.0-3 Axisymmetric Approximation of PF1 Coils and Support Structure

(Evolution of structure incorporates outer bands to the PF1a and 1b mandrels)
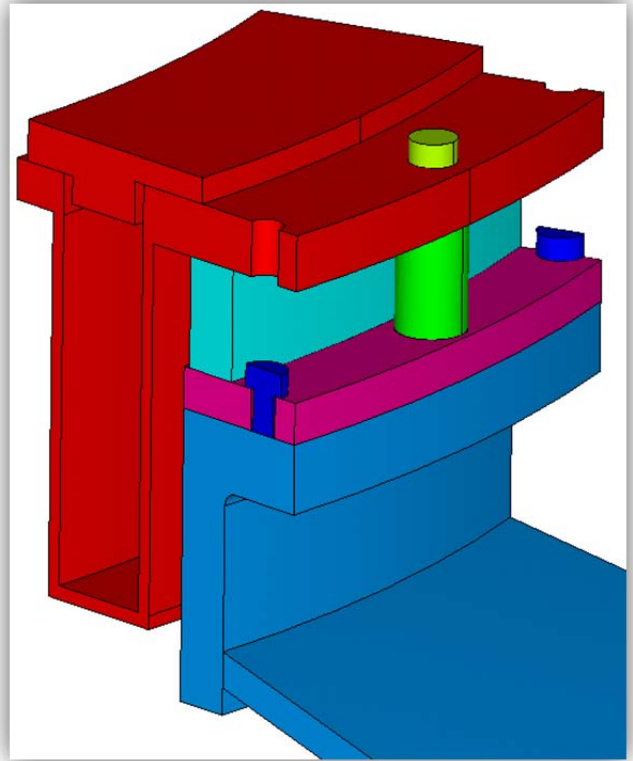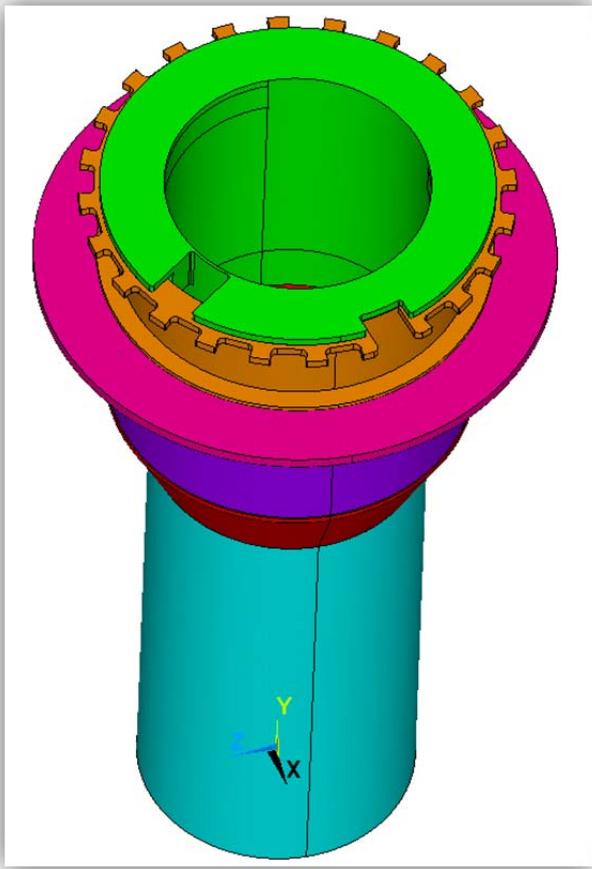
Fig. 4.0-4 Examples of 3D Modeling Details

4.1 Analysis Nomenclature and Nominal Stress Limits

EM field and structural models are performed in SI units. It may be helpful to list typical SI units and conversion factors for those more familiar with English units. It is also helpful to have stress limits in mind when reviewing stress results. Here are some useful units, conversions and stress limits:

SI units and conversions:

> Flux Density [T]
> Displacement [m]
> Stress [Pa], 0.145 ksi/MPa
> Force [N], 0.2248 lb/N, 1 kip =1000 lb

Cu conductor used in the PF coils will have hardness similar to that of the TF conductor

> S_y = 262 MPa
> S_m = (2/3) S_y = 174 MPa
> Membrane + Bending Stress Limit at RT: (1.5) S_m = 262 MPa
> Membrane + Bending Stress Limit at 100C: (temp reduction factor 0.9) (1.5) S_m = 236 MPa
> Cyclic Max Stress Limit (100ºC) = 125 MPa (limit established by P. Titus, "OH Conductor Fatigue Analysis," NSTXU-CALC-133-09-00 Rev 0, Nov 2010)

Center stack coil support structure is made from Inconel 625:

> S_y~65 ksi, S_{ut}~130 ksi
> S_m~43 ksi (300 MPa)
> Membrane + Bending Stress Limit at RT: (1.5)300=450 MPa
> Max Cyclic Stress (58.5k cycles) = 375 MPa (R~0.05), see Fig. 4.1-1

Inner PF Coil Mandrels are made from 316SST (ref. ?, Titus' Table 7.1-2 Coil Structure Room Temperature (292 K) Maximum Allowable Stresses):

> S_y=276 MPa, S_{ut}=613 MPa
> S_m=184 MPa (161 MPa for welds)
> Membrane + Bending Stress Limit at RT: (1.5)184=276 MPa (241 MPa for welds)
> Max Cyclic Stress (58.5k cycles) = 350 MPa (R=0), see Fig. 4.1-2

PF coil conductor insulated with Epoxy-Glass (surface prepared and primed)

Ultimate Shear (RT) = 65 MPa (R. P. Reed, "Estimated and Compiled Properties of Glass/101K Epoxy/Kapton Composite Properties at Room Temperature," July 15, 2009)

Ultimate Shear (100ºC) = 51 MPa (CTD, Inc., "Fabrication and Testing of Cyanate Ester-Epoxy/Glass Fiber/Copper Laminates," PPPL PO PE010925-W, Oct. 7, 2011).

Fatigue Shear (85ºC) = 19-30 MPa (CTD ibid)

Shear Stress Limit at 85ºC: τ_0= 2/3(30 MPa) = 20 MPa (also: (~0.6x51)(2/3) = 20 MPa)

Flat-wise secondary tension stress fatigue at 50ºC: 2/3(15 MPa) = 10 MPa (CTD ibid)

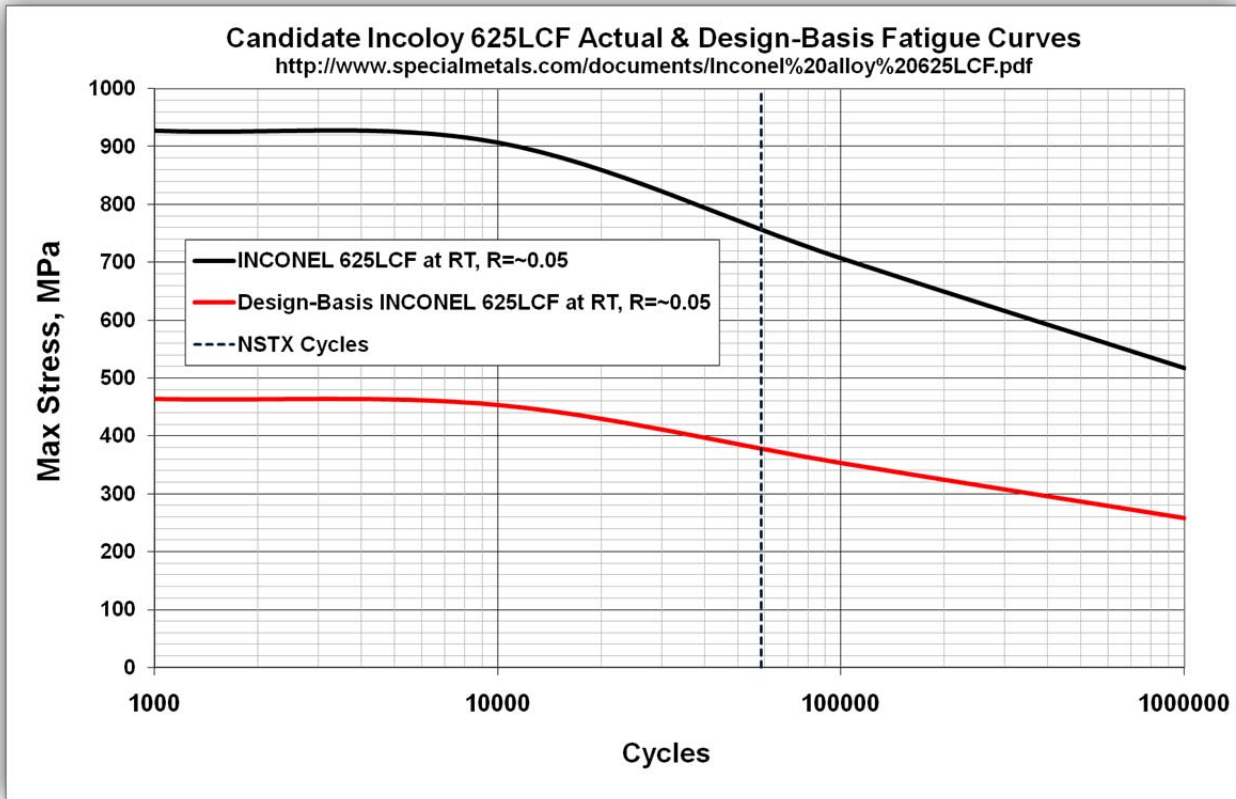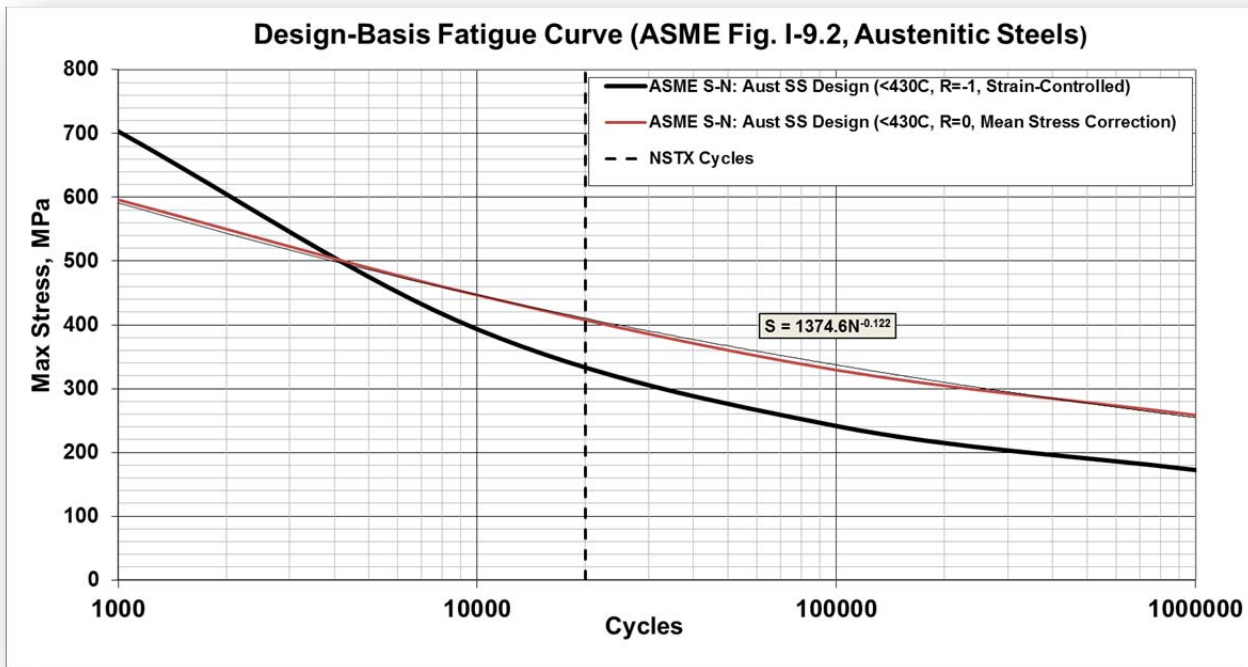Fig. 4.1-1 INCONEL 625LCF Fatigue Curve

Fig. 4.1-2 Austenitic Stainless Steel Fatigue Curve

4.2.1 Design Space Search based on 2D Smeared WP Model

Initially, the 2D field/stress models are based on a smeared WP representation to reduce the analysis time for this scoping study. The max stress in each of the PF1 WPs plus the structures are written to an array for each of these operating conditions. Results are imported into Excel and plotted as bar charts in order to give a simple visual representation. Note that smeared WP stresses must be scaled up to determine Cu stresses (typically <2x, as discussed later).

Fig. 4.2.1-1 shows the max smeared PF1a and 1b WP stress for all 480 operating current equilibria.
> EQ51 produces the highest stress (~20 MPa) in the PF1a WP, shaped plasma.
> EQ3 (&18) produces the highest stress (~25 MPa) in PF1b WP, shaped plasma.

Fig. 4.2.1-2 shows the max stress in the PF1a and 1b coil support structures for all 480 operating current equilibria.
> EQ1 (&16) produces the highest stress (95 MPa) in coil case, Post Circular plasma disruption.

Fig. 4.2.1-3 shows the max smeared PF1c WP (top) and coil case (bot) stresses for all 480 operating current equilibria.
> EQ1 (&16) produces the highest stress (20 MPa) in PF1c WP, Post Shaped plasma disruption.
> EQ1 (&16) produces the highest stress (140 MPa) in coil case, three no-plasma cases.

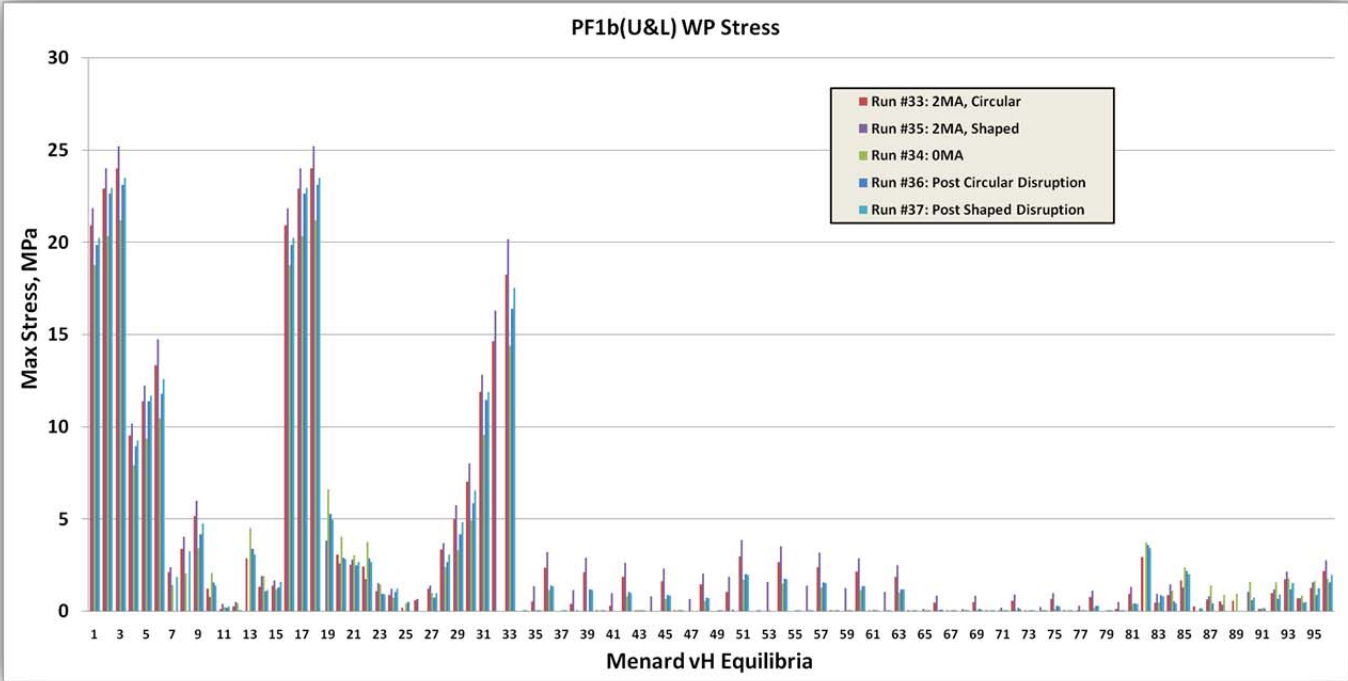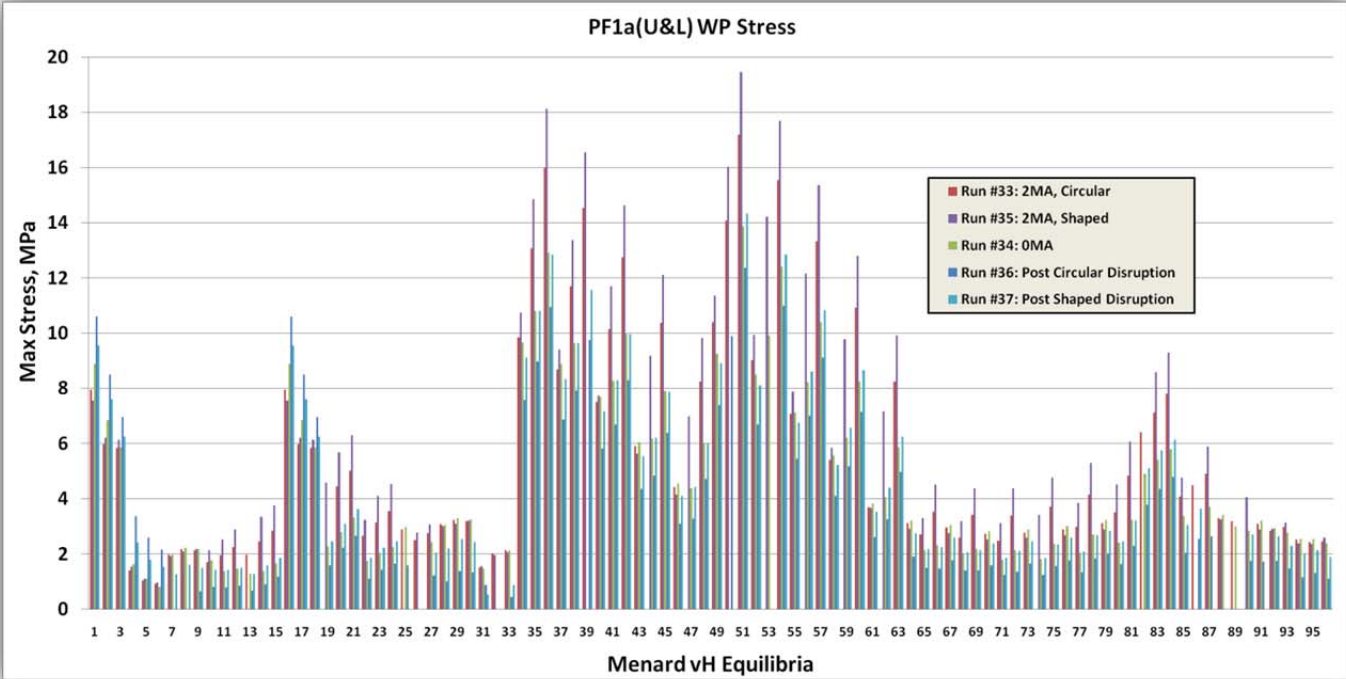Fig. 4.2.1-1 Smeared PF1a (top) and 1b (bot) WP Stress, (96) Equilibria x (5) Plasma Conditions

Fig. 4.2.1-2 PF1a & b Coil Case Stress, (96) Equilibria x (5) Plasma Conditions
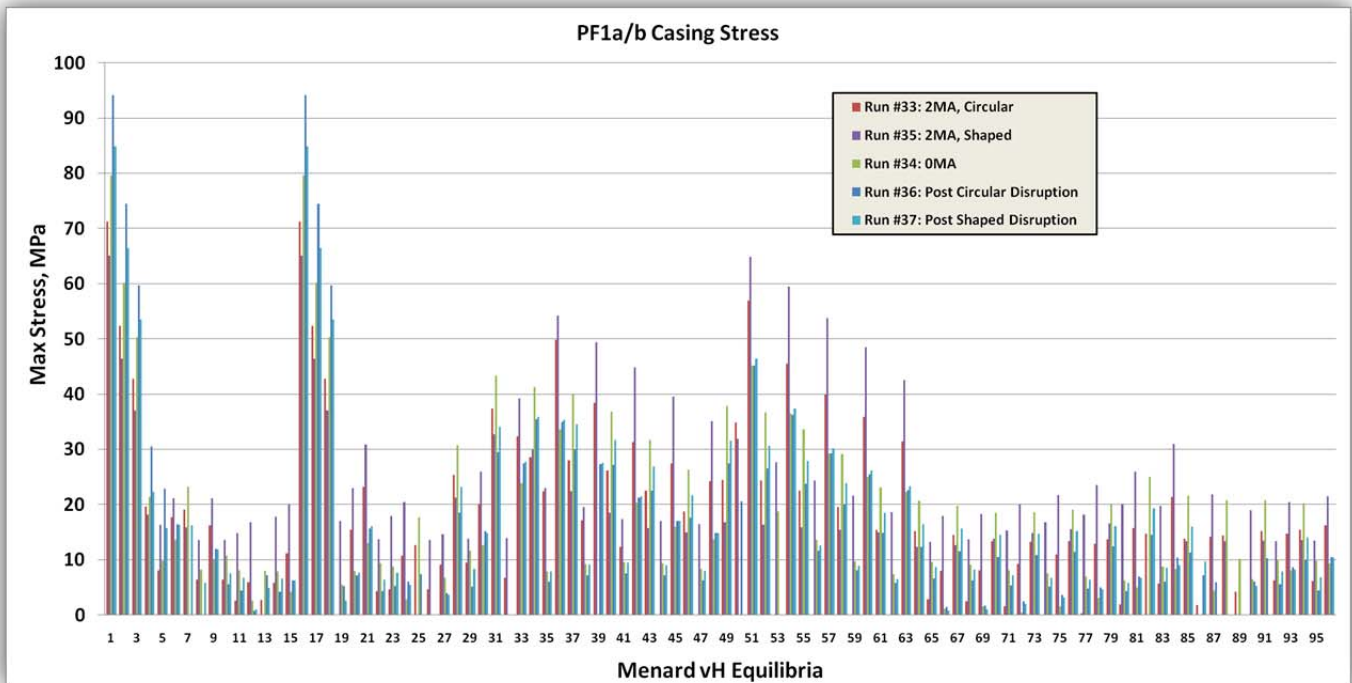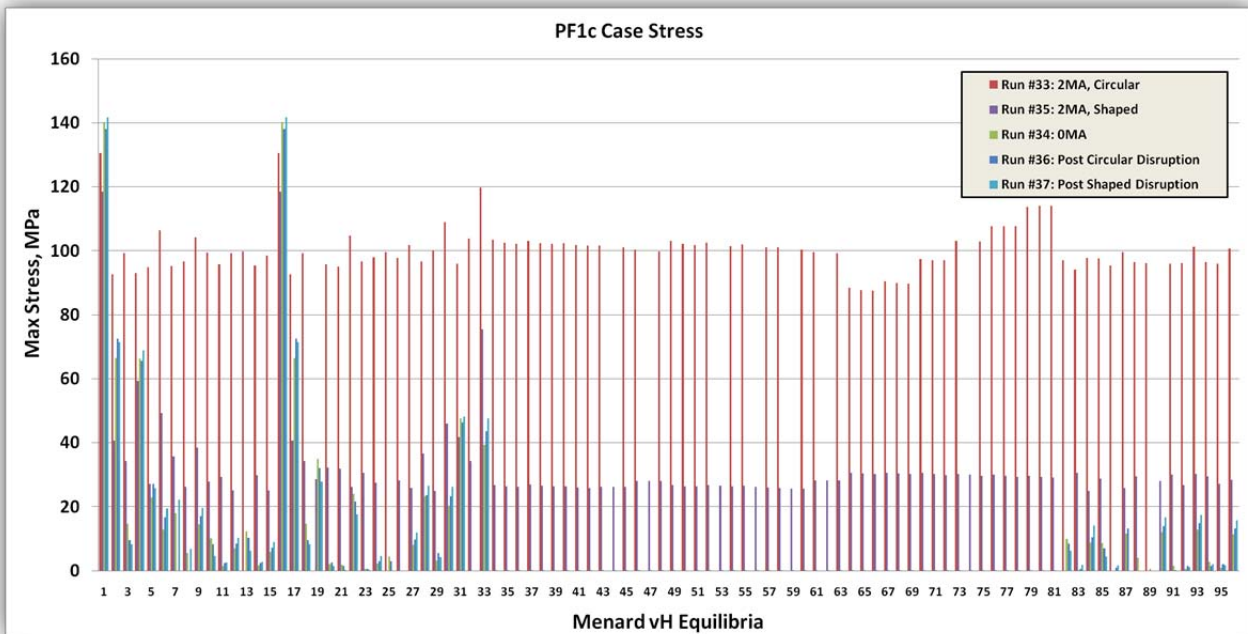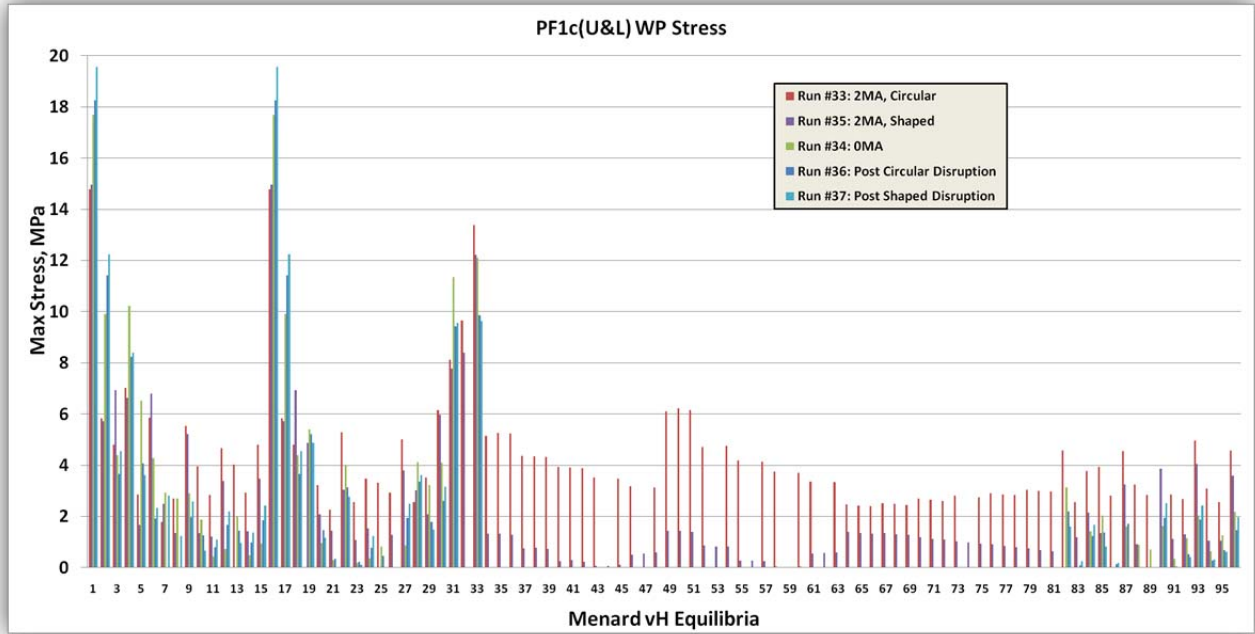
Fig. 4.2.1-3 Smeared PF1c WP (top) and Coil Case (bot) Stress, (96) Equilibria x (5) Plasma Conditions

The "OH_PF_Forces" sheet in the DPS lists the max radial and vertical forces from all equilibria. Focusing on PF1 coils, the max values are highlighted in yellow as shown in Table 4.2.2-1, and their corresponding equilibria are traced back to the "Forces_Circ," "Forces_Shaped" and "PF_Currents_Forces" sheets.

Table 4.2.2-1 Max Radial & Vertical Coil Forces (All scenarios and Plasma conditions)

Fr(lbf)	PF1aU	PF1bU	PF1cU	PF2U	PF3U	PF4U	PF5U	PF5L	PF4L	PF3L	PF2L	PF1cL	PF1bL	PF1aL
Min w/o Plasma	-35364	-5460	-71314	-81887	-81302	-95014	82098	82131	-95015	-40089	-81885	-71290	-5460	-35367
Min w/Plasma	-86091	-3452	-51380	-47307	-69284	-105829	153489	153522	-105833	-36766	-47306	-51356	-3452	-86092
Min Post-Disrupt	-56775	-1387	-49577	-55731	-54657	-152166	37239	37254	-152181	-54655	-55729	-49552	-1387	-56777
Min	-86091	-5460	-71314	-81887	-81302	-152166	37239	37254	-152181	-54655	-81885	-71290	-5460	-86092
Worst Case Min	-308932	-259553	-280590	-257217	-188584	-147049	-20978	-20974	-147050	-188591	-257215	-280542	-259506	-308941
Max w/o Plasma	244828	141199	12805	98896	237654	260114	507319	507406	260110	237644	98897	12806	141221	124108
Max w/Plasma	390442	176824	17578	78348	228719	289472	625160	625247	289442	228730	78348	17561	176800	221474
Max Post-Disrupt	271221	159652	18316	69039	165064	122372	370962	371032	122359	165058	69040	18297	159632	139721
Max	390442	176824	18316	98896	237654	289472	625160	625247	289442	237644	98897	18297	176800	221474
Worst Case Max	1202680	427957	291802	298121	474283	468175	667690	667786	468173	474271	298121	291843	427989	1202670

Fz(lbf)	PF1aU	PF1bU	PF1cU	PF2U	PF3U	PF4U	PF5U	PF5L	PF4L	PF3L	PF2L	PF1cL	PF1bL	PF1aL
Min w/o Plasma	-80237	-34659	-18534	-40938	-138527	-203125	-239984	-49657	-78008	-29737	-47150	-58912	-84182	-42574
Min w/Plasma	-71687	-49080	-32610	-51374	-65903	-171261	-150401	-145159	-63458	-12660	-35660	-50407	-78646	-31269
Min Post-Disrupt	-95770	-33155	-22126	-32928	-94339	-89099	-203129	-18322	-134053	-43904	-47032	-59782	-83221	-35298
Min	-95770	-49080	-32610	-51374	-138527	-203125	-239984	-145159	-134053	-43904	-47150	-59782	-84182	-42574
Worst Case Min	-169764	-204276	-126322	-149606	-291685	-415945	-507307	-181134	-74599	-218764	-152079	-114523	-139881	-300586
Max w/o Plasma	53473	84182	58912	47150	98898	78008	49657	239984	180293	138527	40093	18534	34659	80236
Max w/Plasma	37012	78647	50408	35661	52893	63458	145158	150401	148418	65903	55892	32609	49080	71686
Max Post-Disrupt	46450	83220	59782	47033	92132	134052	18321	203130	89100	94339	37985	22125	33155	95770
Max	53473	84182	59782	47150	98898	134052	145158	239984	180293	138527	55892	32609	49080	95770
Worst Case Max	300589	139882	114523	152080	218764	149102	181376	507307	415946	291685	149636	126322	204275	118263

4.2.3 Summations of Vertical Forces for Grouped Coils

A review of the inner PF coil structural load path shows that certain coil groupings, when considered together, can contribute to the maximum attractive or repulsive loads. These max load summation conditions are also tracked back to specific equilibria in the DPS, and identified as *ANSYS Time* 1-14.

- ➢ "PF1aU+PF1bU"
- ➢ "PF1aU-PF1bU"
- ➢ "PF1aL+PF1bL"
- ➢ "PF1aL-PF1bL"
- ➢ "(PF1aU+PF1bU)+(PF1aL+PF1bL)"
- ➢ "(PF1aU+PF1bU)-(PF1aL+PF1bL)"

Table 4.2.3-1 (14) Critical EQs Based on Max Coil Forces (Single and Grouped)

Spreadsheet Tab	Plasma	EQ#
PF_Current_Forces ANSYS TIME: 1-8	0 MA	1,3,31,33,34,51,52,84
Forces_Shaped ANSYS TIME: 9-13	2 MA	18,33,51,54
	Post-Disruption	3
Forces_Circ ANSYS TIME: 14	Post-Disruption	1

4.2.4 Enveloping Equilibria of Interest

The most important operating points (equilibria) based on all of the stress scoping and net coil force screening techniques discussed above are consolidated into Table 4.2.4-1. We see that the 480 equilibria can be enveloped by just 10. Each of these operating conditions is evaluated with the 2D model, but with the WP conductors and insulation modeled explicitly (not smeared). Notice that the bottom row reflects the summary of all 96 equilibria with a 2MA *shaped* plasma. This approach is not repeated for the other four plasma conditions, just the few equilibria which are caught by the screening approach.

Table 4.2.4-1 2D Stress Results from Most Important Equilibria

Time Point	SI(Casing)	SI(1aU/L)	SI(1bU/L)	SI(1cU/L)	EQ# (Spreadsheet Tab)
1	80.1	18.0	26.8	30.6	#65 (PF_Currents_Forces)
2	24.4	3.1	21.0	15.8	#97 (PF_Currents_Forces)
3	41.5	14.3	1.1	0.0	#98 (PF_Currents_Forces)
4	36.9	12.6	0.1	0.0	#116 (PF_Currents_Forces)
5	7.4	9.2	1.6	2.6	#148 (PF_Currents_Forces)
6	36.9	9.4	32.7	10.8	#195 (Forces_Shaped) & 3 of 96
7	40.0	2.8	28.1	20.8	#210 (Forces_Shaped)
8	64.9	29.2	7.6	2.5	#228 (Forces_Shaped) & 51 of 96
9	59.4	26.5	7.0	1.6	#231 (Forces_Shaped)
10	94.6	21.6	27.9	31.2	#290 (Forces_Circ), post-disrupt
1-96	65.6	29.4	32.7	29.3	Max of 1-96 (2 MA Shaped Plasma)

4.3 Stress Results: Axisymmetric Modeling

4.3.1 Worst PF1a/1b Mandrel Stress

Both smeared WP stress and force summation screening tools have accurately pointed to the highest stress-producing equilibrium for the 316SST coil mandrels: EQ1, Post Circular Disruption (TIME=14), when PF1aU pushes down (-96 kip) and PF1bU pushes up (83 kip). As shown in Fig. 4.3.1-1, this develops a maximum stress of 140 MPa in the PF1a mandrel.

Enveloping Static and Fatigue Evaluation:
- Local M+B<140 MPa <276 MPa
- Total Stress=140 MPa <350 MPa
- Static & Fatigue: Qualified
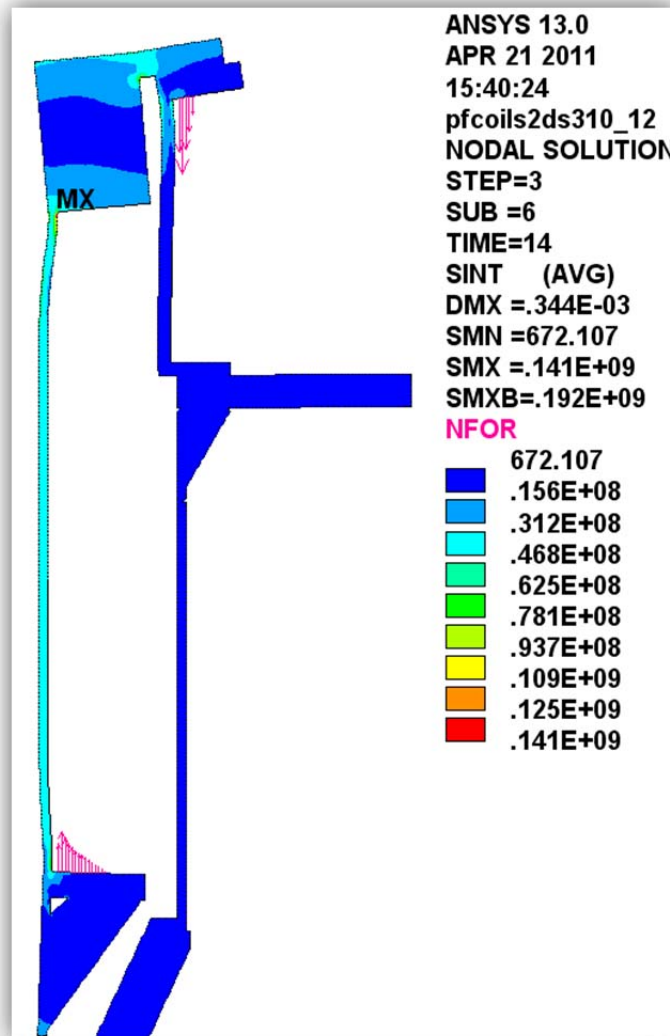
Fig. 4.3.1-1 Max PF1a/b Mandrel Stress

4.3.2 Worst Weld Stress

The max stress in the welds is produced by EQ31 (TIME=3). During this equilibrium, the max separating force 56 kip as defined by Fz(1aU & 1bU)-Fz(1aL & 1bL). As shown in Fig. 4.3.2-1, the resulting maximum stress of 50 MPa occurs in the Inconel 625 welds.

Enveloping Static and Fatigue Evaluation:
- Local M+B<50 MPa < (1.5 x Weld reduction factor 0.875 x 300 MPa = 390 MPa)
- Total Stress=50 MPa < 375 MPa
- Static & Fatigue: Qualified
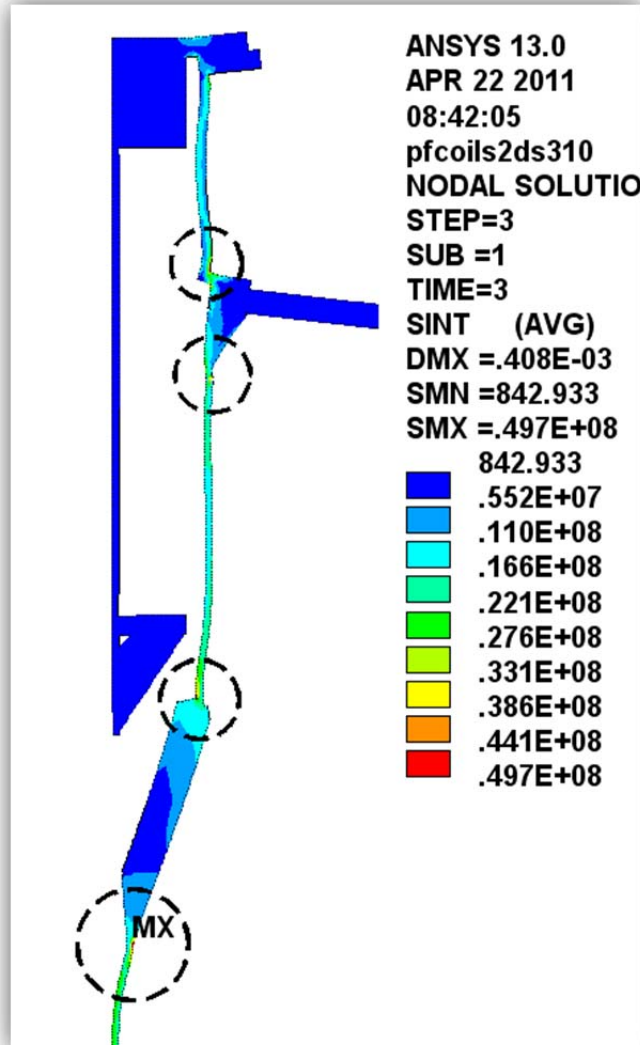
Fig. 4.3.2-1 Max Structural Weld Stress

4.3.3 Worst PF1c Case Stress

EQ1 (TIME=1) produces the largest (60 kip) vertical load on the PF1c coils (pushed away from the mid-plane). As shown in Fig. 4.3.3-1, the simple restraint at the flange OD and the idealized cover/flange bond here in the 2D model results in a cover plate stress of 200 MPa.

Enveloping Static and Fatigue Evaluation:
- Local M+B<202 MPa<276 MPa
- Total Stress=202 MPa<350 MPa
- Static & Fatigue: Qualified
- 3D model will provide greater accuracy in this region.
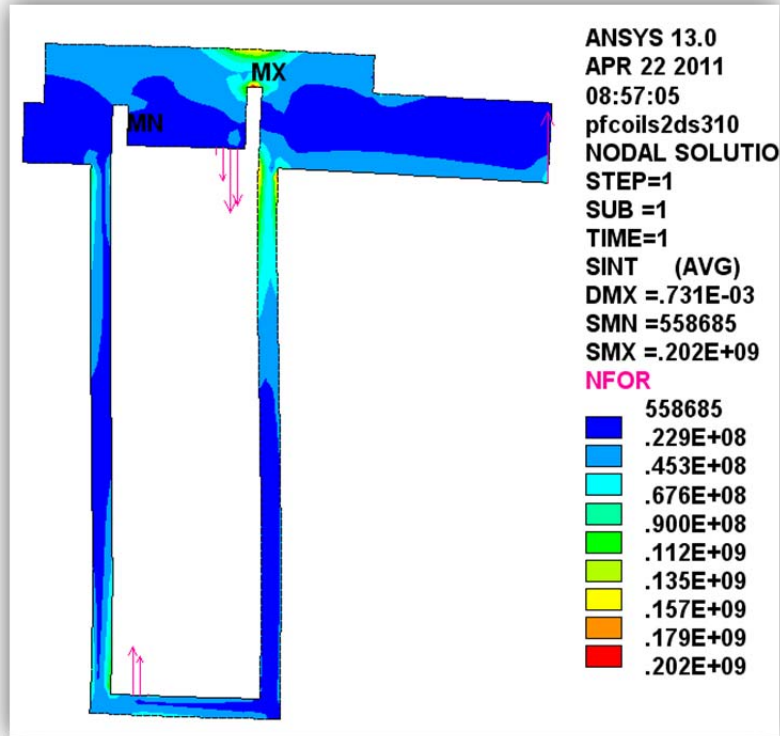
Fig. 4.3.3-1 PF1c Case Stress

4.3.4 PF1a Cu Max Hoop & Tresca Stress

EQ51 (TIME=11) produces the largest radial force in PF1aU (390 kip). This results in the largest PF1a hoop stress of 17 MPa as shown in the Fig. 4.3.4-1 (left) contour plot.

EQ54 (TIME=12) also produces a relatively large radial force in PF1aU (355 kip). This loading results in the largest PF1a Tresca stress of 30 MPa as shown in the Fig. 4.3.4-1 (right) contour plot. Here, the Tresca stress is driven mostly by a vertical stress amplified by the cooling channel hole.

Enveloping Static and Fatigue Evaluation:
- Local M+B <30 MPa <236 MPa
- Total Stress =30 MPa <142 MPa
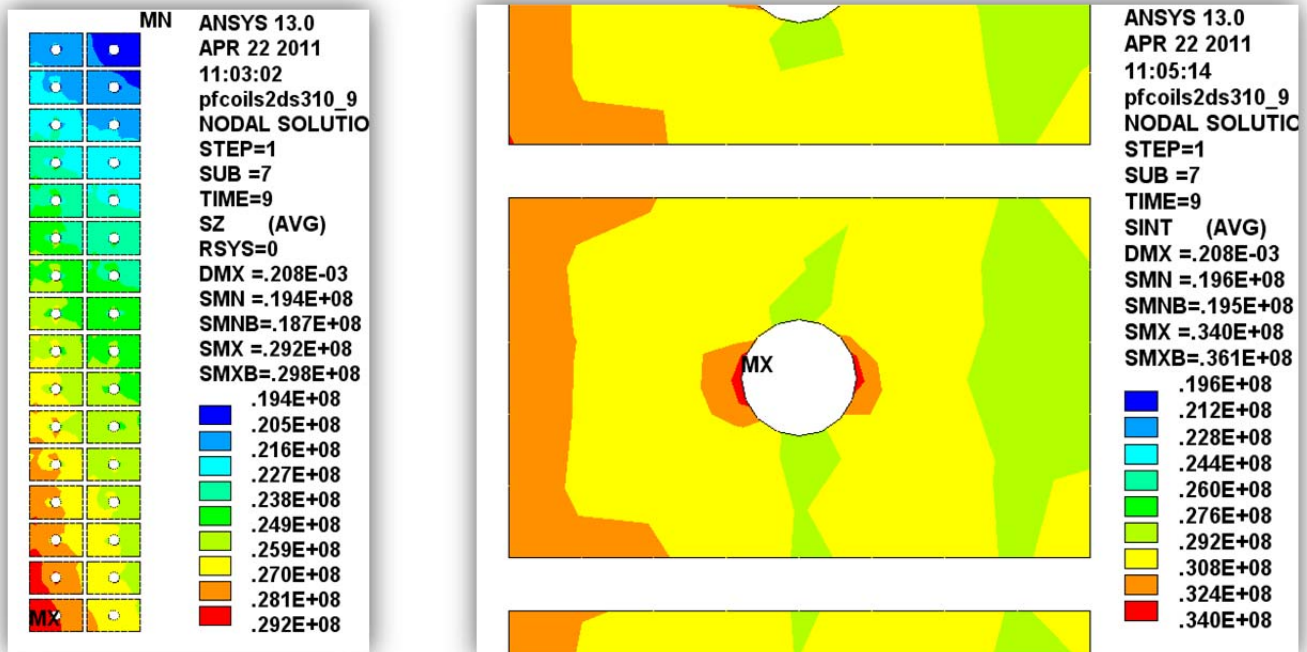- Static & Fatigue: Qualified
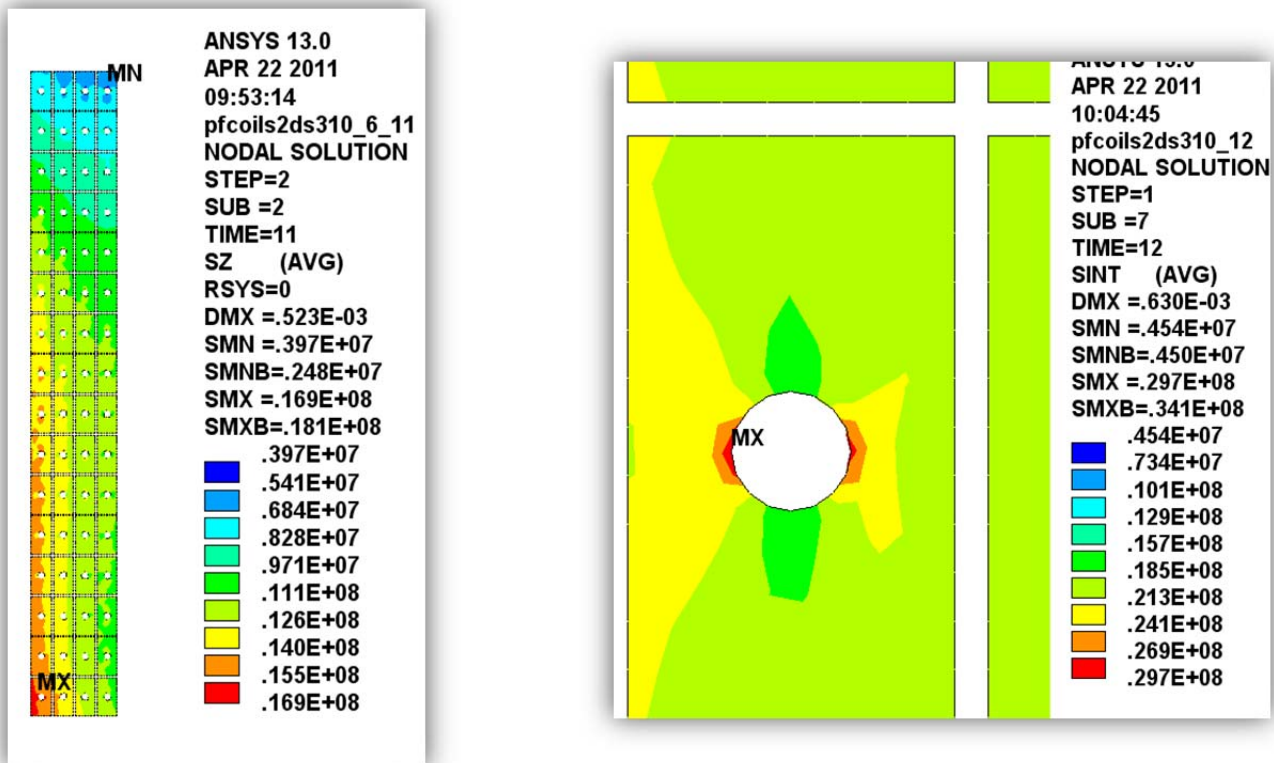
Fig. 4.3.4-1 PF1a Cu Hoop and Tresca Stresses

4.3.5 PF1a Insulation Max Compression & Shear Stress

The post-disruption of a circular plasma from EQ1 (TIME=14) produces the max PF1aU downward load (-96 kip) and results in the largest compressive stress in the insulation. As shown in Fig. 4.3.5-1, local compressive stresses reach -14 MPa, which are very low for any epoxy-glass insulation system (typical limited to 180 MPa). Coil deformations also produce a 1-3 MPa secondary normal tensile stress, which is below the 10 MPa limit.

The shear stress in the PF1a insulation is also a max at this time point. At 2.6 MPa, it is well below the 20 MPa shear stress limit.
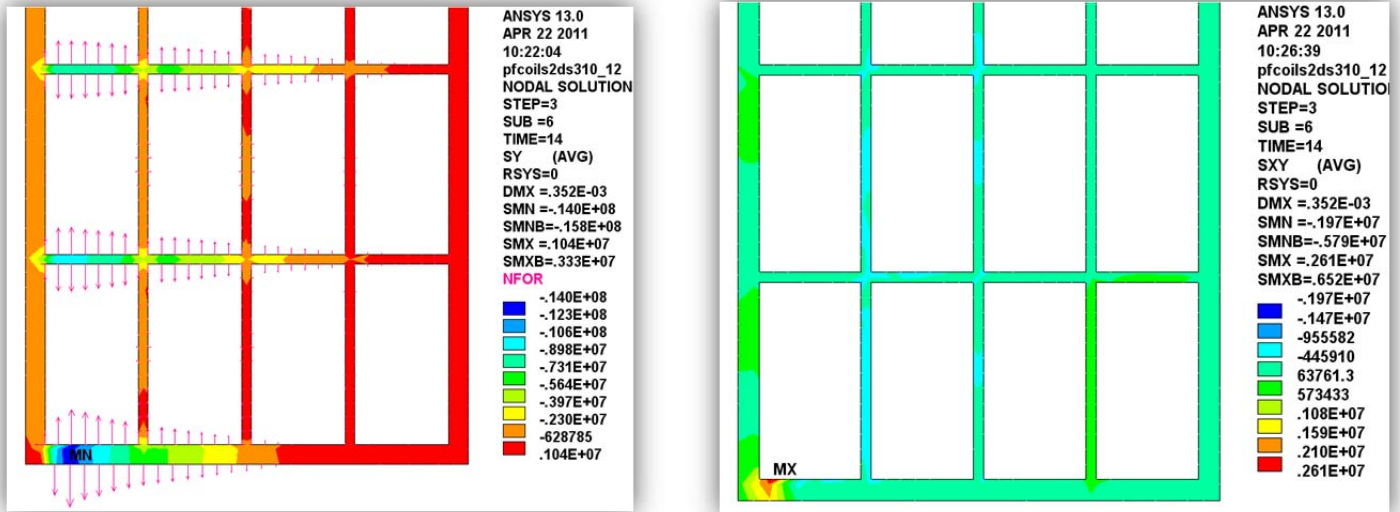
Fig. 4.3.5-1 Insulation Normal and Shear Stress

4.3.6 PF1b Cu Max Hoop & Tresca Stress

EQ18 (TIME=9) produces the largest radial force in PF1b (177 kip), which results in the largest hoop stress of 29 MPa as shown in the Fig. 4.3.6-1 (left) contour plot.

EQ18 also produces the largest Tresca stress of 34 MPa as shown in the contour plot on the right (24 parts hoop tension and 10 parts vertical compression).

Enveloping Static and Fatigue Evaluation:
- Local M+B <34 MPa <236 MPa
- Total Stress =34 MPa <142 MPa
- Static & Fatigue: Qualified

Fig. 4.3.6-1 PF1b Cu Max Hoop & Tresca Stress

4.3.7 PF1b Insulation Max Compression & Shear Stress

The post-disruption of a circular plasma from EQ1 (TIME=14) produces the 2nd largest PF1bU upward load (83 kip, 84 kip when Ip=0) and results in the largest compressive stress in the insulation. As shown in Fig. 4.3.7-1, local compressive stresses reach -19 MPa (typical limited to 180 MPa). Coil deformations also produce a 1.8 MPa secondary normal tensile stress, which is below the 10 MPa limit.

The shear stress in the PF1b insulation is also a max at this time point. At 4 MPa, the shear stress is well below the 20 MPa limit.
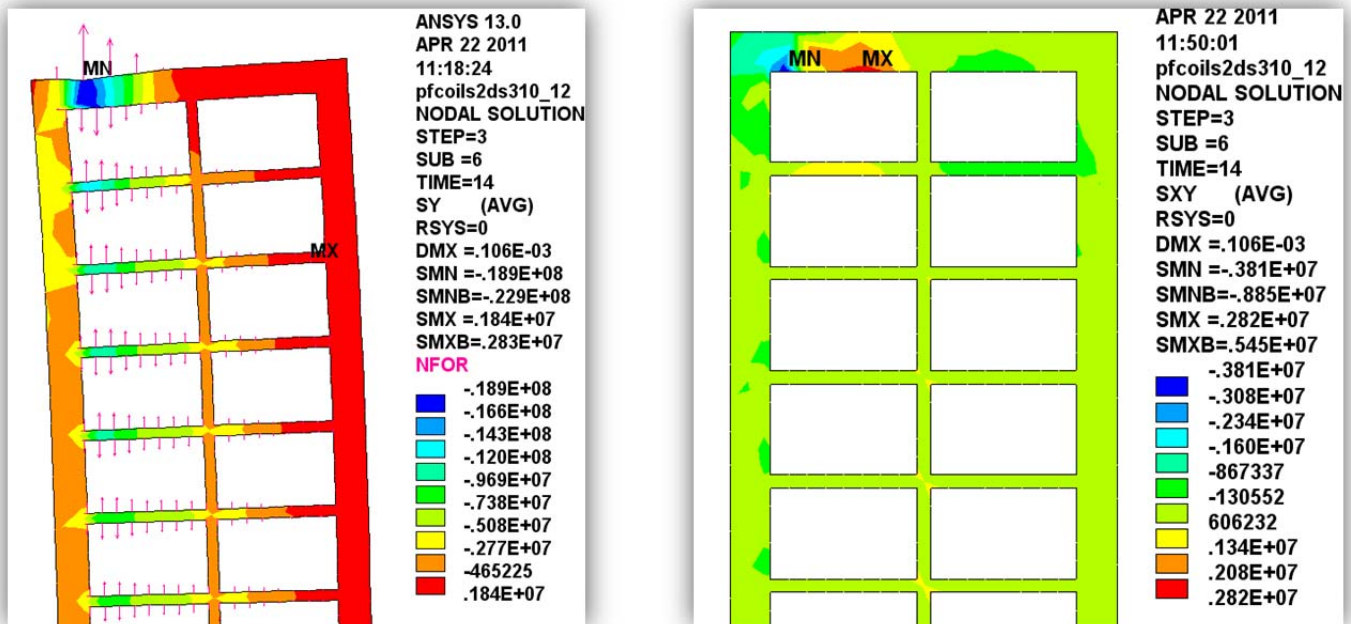
Fig. 4.3.7-1 Insulation Normal and Shear Stress

4.3.8 PF1c Cu Max Hoop & Tresca Stress

While EQ33 (0 MA plasma) produces the largest net radial force in PF1c (-71 kip) while EQ1 (TIME=1) produces the largest and smallest hoop stresses. As shown in Fig. 4.3.8-1 the hoop stress ranges from -24 to +14 MPa. This same EQ1 also produces the largest Tresca stress, 36 MPa, predominantly due to a local contact stress.

All stresses are well below the enveloping fatigue limit of 142 MPa, which implicitly qualifies the Cu for static and fatigue requirements.
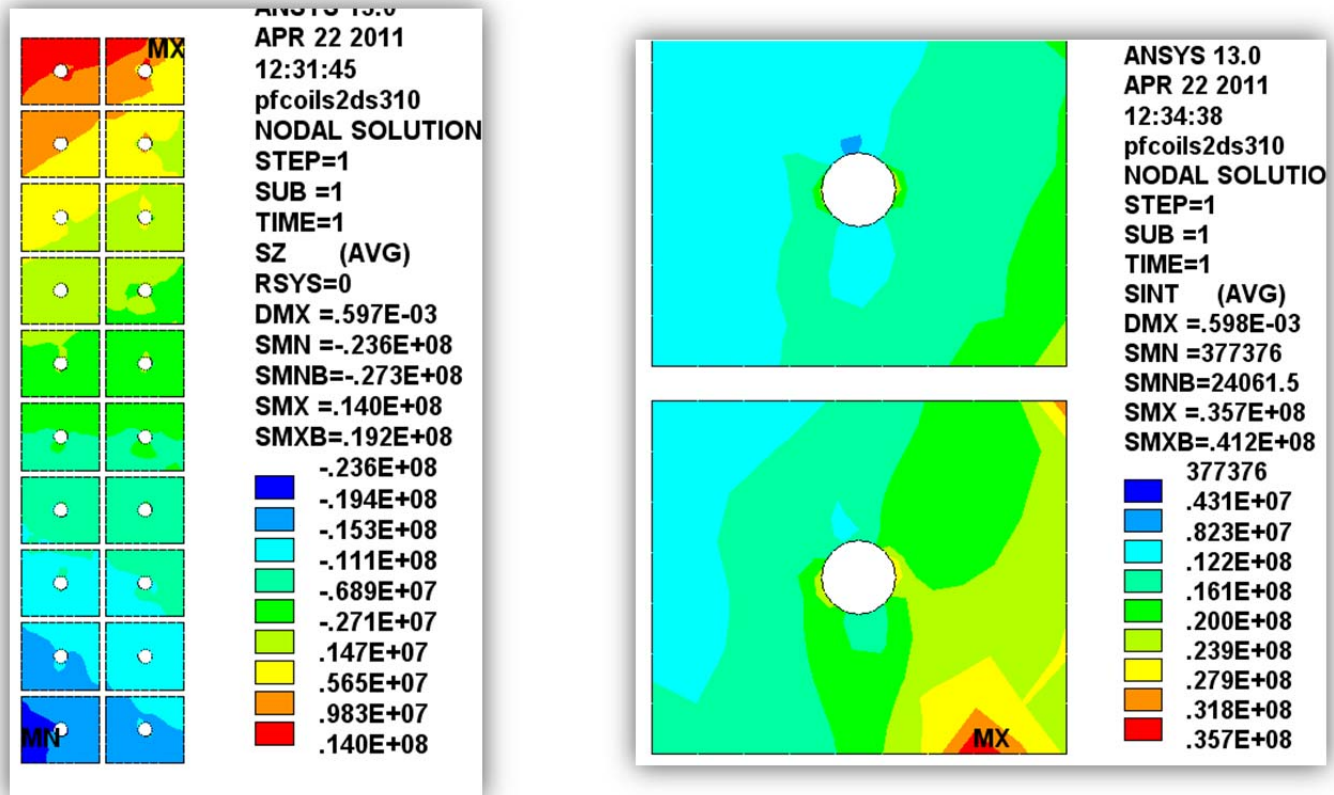
Fig. 4.3.8-1 PF1c Cu Max Hoop & Tresca Stress

4.3.9 PF1c Insulation Max Compression & Shear Stress

EQ1 (TIME=1) produces the largest PF1c repulsive loads (~60 kip) whenever Ip=0, and results in the largest compressive stress in the insulation. As shown in Fig. 4.3.9-1, the max compressive stress is -40 MPa (typical limited to 180 MPa). Coil deformations also produce a 2 MPa secondary normal tensile stress, which is below the 10 MPa limit.

The shear stress in the PF1c insulation is also a max at this time point. At 8 MPa, the highly localized max shear stress is still well below the 20 MPa limit.
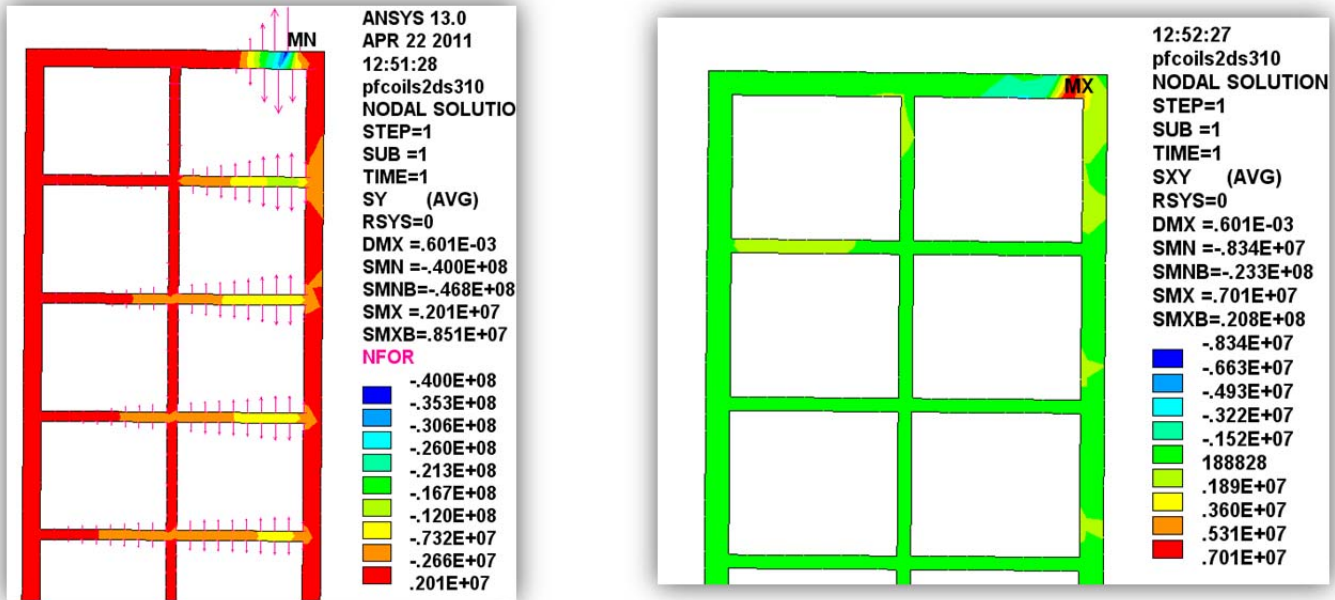
Fig. 4.3.9-1 PF1c Insulation Max Compression & Shear Stress

4.3.10 Radial Displacements

The enveloping 14 cases are also reviewed for max radial displacements. As shown in the contour plot of Fig. 4.3.10-1 (left), the worst case radial deflection of <0.1 mm occurs in PF1b at "TIME"=9 (EQ18, 2MA shaped plasma).

When unrestrained thermal expansion effects are added to the analysis (PF1a at 85C, PF1b & 1c at 100C), the radial displacements are as shown in the plot on the right. Thermal strains are calculated assuming a 150ºC (zero strain) reference temperature. The relative motion between structure and coil WP are:

- $\Delta r(PF1a) = 0.5$ mm
- $\Delta r(PF1b) = 0.7$ mm
- $\Delta r(PF1c) = 1.1$ mm (will be constrained by the mechanical continuity with the coil case)

EM Only   EM + Max Operating Temp
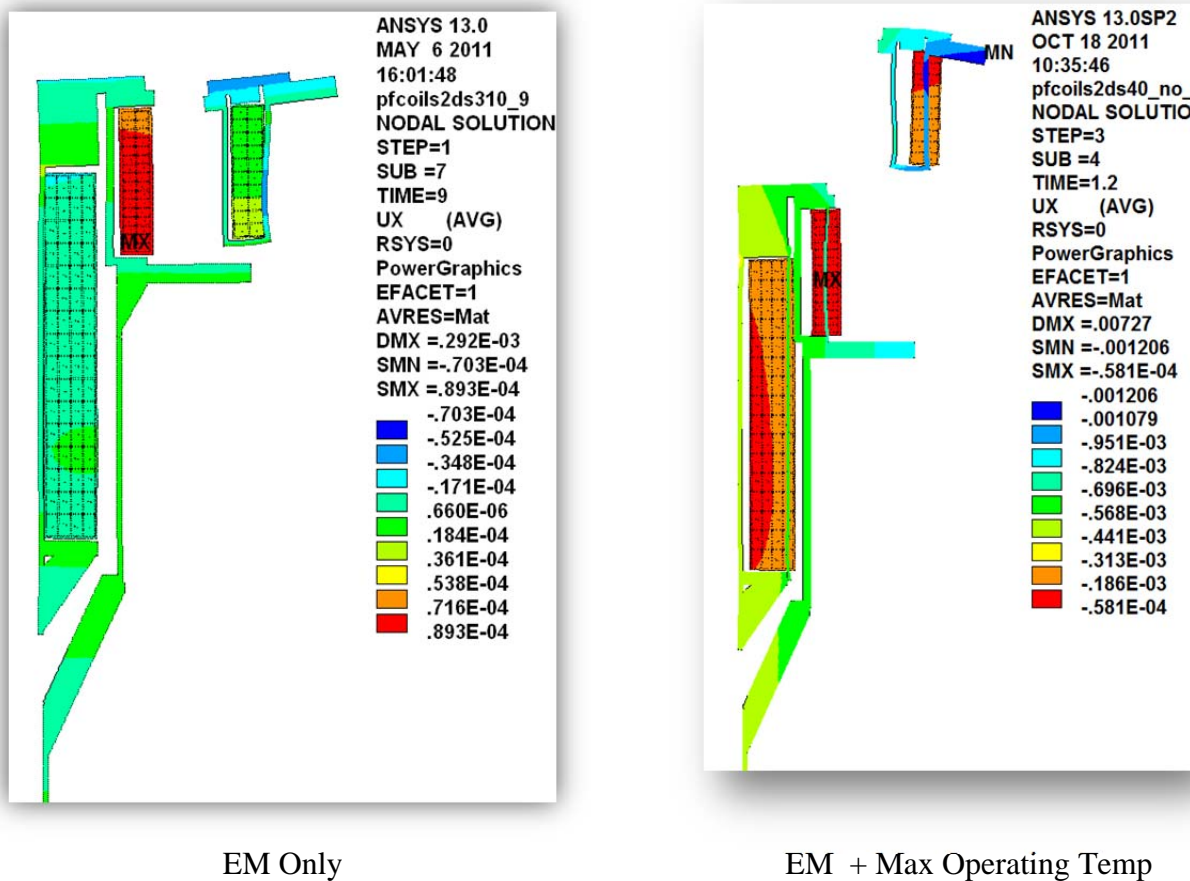
Fig. 4.3.10 Radial Displacements

4.3.11 Thermal Expansion Stress Analysis

The coils are VPI'd and cured at 170°C but don't develop full mechanical stiffness until cooled below ~150°C (ref. P. Fabian, CTD, Inc.). During operation, the PF1b/1c coils are expected to reach 100°C, while PF1a warms to 85°C. The thermal growth (δ_{th}) of the warm/largest PF1c coil within its actively cooled mandrel is estimated as follows:

$$\delta_{th}(radial)=(r=0.4m)(\alpha=16\times10^{-6})(\Delta T=100-25)=0.5 \text{ mm}$$

However, there is some thermal preloading upon cool-down from the cure temperature which will reduce this 0.5 mm value.

The addition of 1/8" external bands to 1a & 1b close the open section formed by the winding mandrel and reduce the thermal expansion effects (assuming no clearance between the coil and band). As shown in Fig. 4.3.11-1, when the coil packs are warmed to their end of pulse temps, they move radially outward while the cases remain at RT. The coils expand radially against the 1/8" outer band which produces a very large (1 GPa) stress in the welds. This is not acceptable.

Conclusion: Some relief at the WP OD/Band interface is required to relieve this structural interaction.
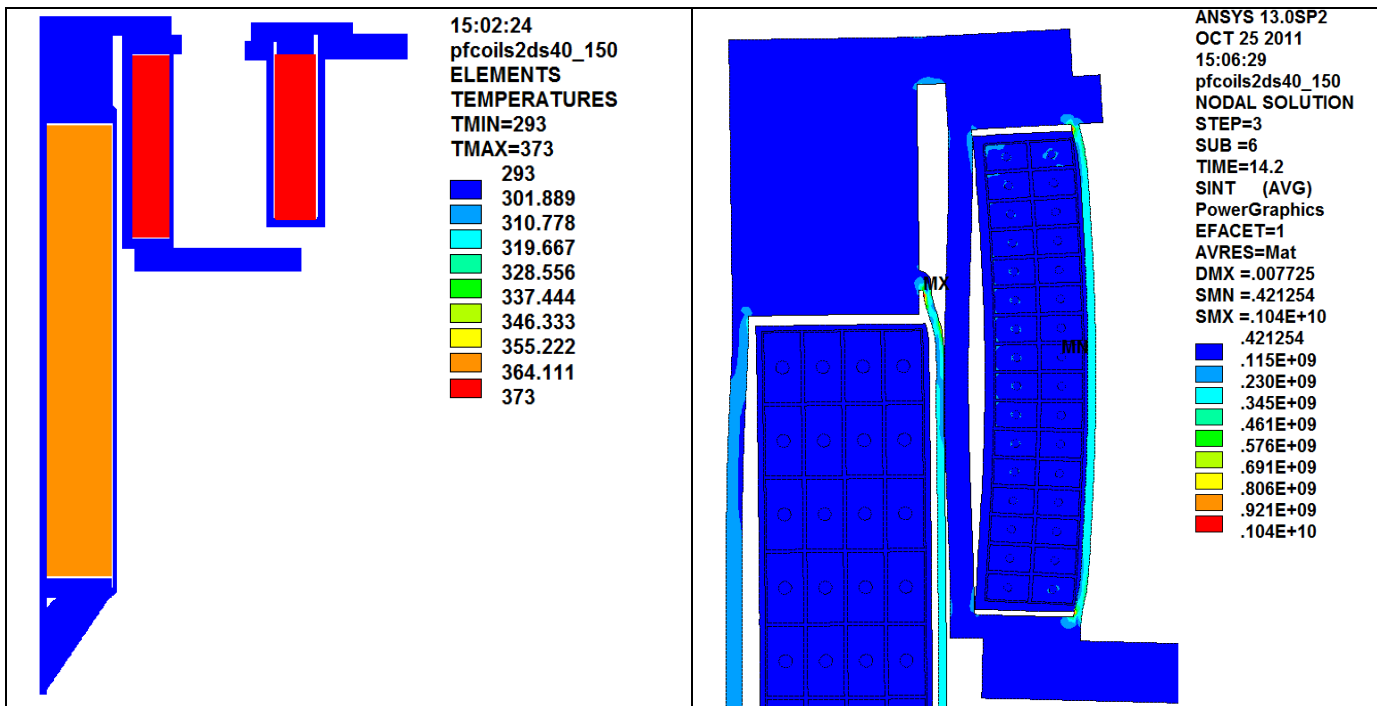
Fig. 4.3.11-1 Max Operating Temperature (left) and Thermal Stress Range from Expansion (right)

Thermal Expansion Effects (Localized Radial Contact between Coil and OD Band)

When a radial gap is provided over all but a few cm at the mid-height of the WP/band interface and thermal expansion effects are added, the warm coil pushes against the top and bottom mandrel flanges stretching the inner shell and outer band. The coil also moves radially away from the inner shell (~0.5 mm) and engages a localized region of the outer band. In the case illustrated in Fig. 4.3.11-3, a heavy band to flange weld carries a local stress of ~200 MPa, down substantially from the 1.0 GPa result. This design feature produces acceptable stress levels while allowing the bands to serve their intended purpose: close the open section formed by the mandrel flanges (essential for PF1a, valuable for PF1b) and maintain radial registration of the WP. Asymmetric coil motions are minimized by the OD bands and the mandrel's ID cylinder (bobbin). Following the current pulse and resulting temperature rise, the re-cooled coil will return to rest against the bobbin.

Fig. 4.3.11-2 Exaggerated Displacements Highlighting Outer Bands Locally Restraining WP
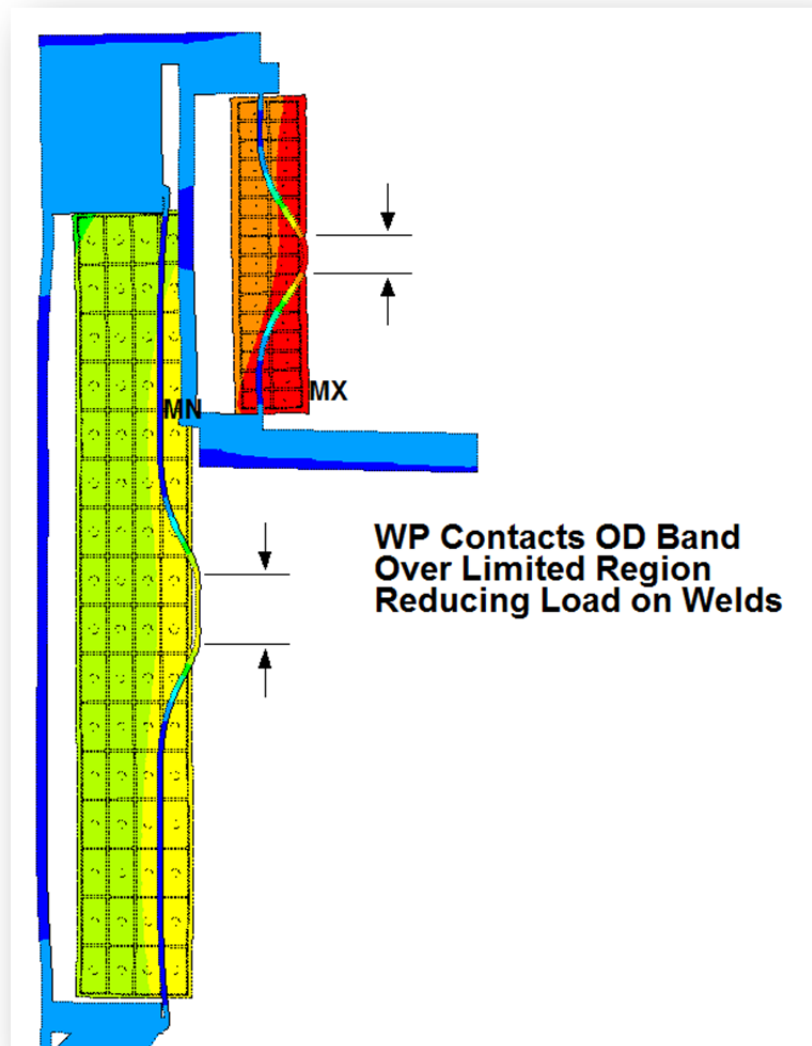
Results indicate acceptable stress levels for a 316 SST band weld.

- Local Mem: 181 MPa (<1.5x161=242 MPa)
- M+B+Q: 204 MPa   (<3.0x161=483 MPa)

Fig. 4.3.11-3 Vertical Stress in PF1a Outer Band to Mandrel Flange Weld
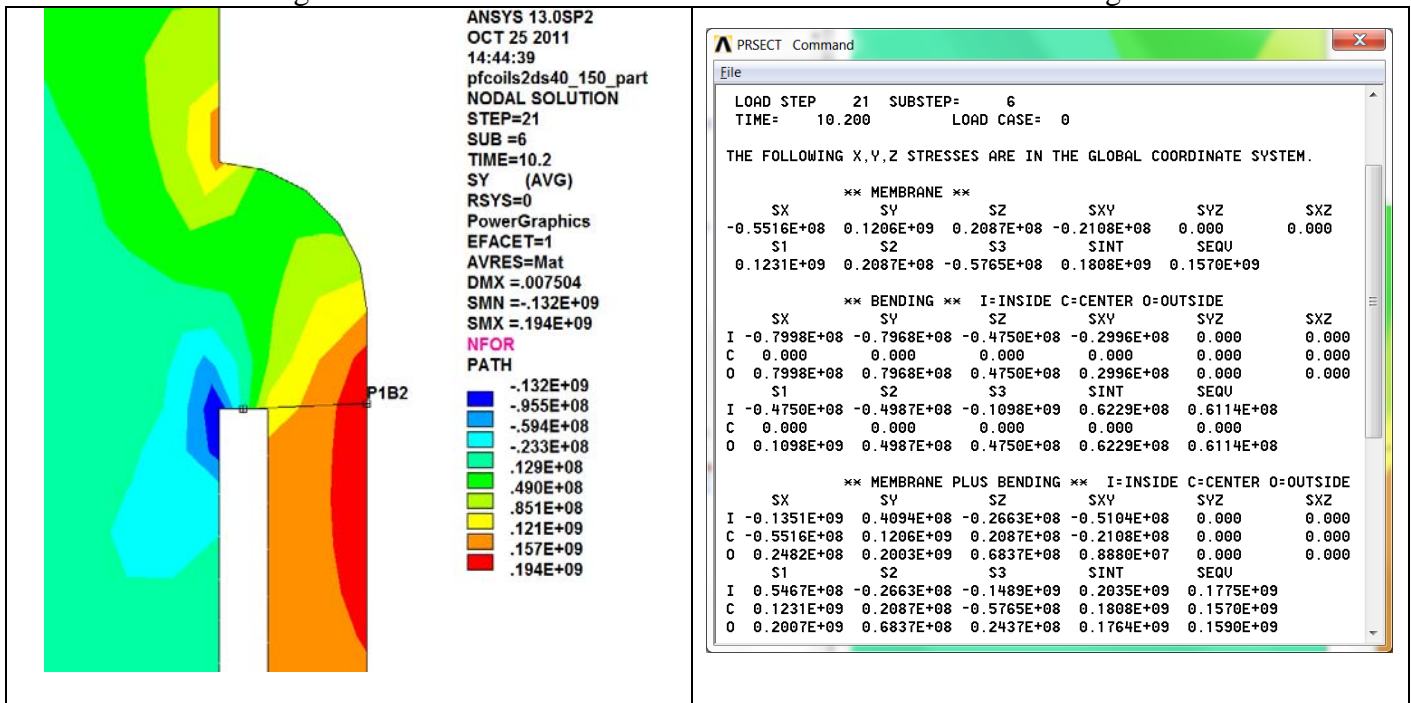
Survey of EM Plus Thermal Expansion Effects

The updated 2D model with closure bands on PF1a and 1b is used to evaluate the effects of all 14 enveloping EM equilibria time points (EQ*) and the added effects of thermal expansion to the coil operating limits (85C for PF1a, and 100C for PF1b/1c). A series of bar charts is included to show the effect of EM loads and EM plus max operating temperature on various coil stresses. In each of these charts, the EQ time point is referred to as number 1-14 corresponding to the critical equilibria listed in Table 4.2.3-1. Analyses are executed for EM loading (denoted EQ#.1) and EM plus max operating temperature (denoted EQ#.2). Because of the X-axis scale, the *.2 labels are not listed, but are represented by the columns of data following the *.1 labels. Stresses in the Cu and SS structure are invariably higher when thermal expansion effects of the warm, end of pulse operating condition are included in the analysis.

Fig. 4.3.11-4 shows a summary of the Cu stresses from these 14 critical equilibria. While the max Tresca stress from EM loading (i.e., early in the pulse) is <40 MPa (EQ#.1 bars), the stress increases to ~130 MPa in PF1c due to the 100C operating temperature and the radial constraint caused by the coil case (second set of bars). These results are illustrated by the two contour plots of Fig. 4.3.11-5 which show that the large Tresca stress in PF1c (right plot) is predominantly due to hoop compression (right plot). Notice that the other coils have light hoop tension since there is minimal OD structure to restrain their thermal growth.

Similarly, the max stress in the 316SS coil case structures is presented in Fig. 4.3.11-6 for all (14) equilibria times two thermal cases per EQ. And again, stresses from just EM loads produces modest stress levels (<170 MPa). With Sm of 184 MPa, all of these EM load cases pass the MEM stress limit without averaging across the section. However, when thermal expansion effects are included, the closed coil cases interact strongly with the warm coils to produce some significant local bending stresses, particularly in PF1c. Each coil support structure is discussed below:

> PF1a: Fig. 4.3.11-7 shows the stress in the PF1a coil support structure for EM EQ10 and a WP temperature of 85ºC. Notice that the max stress is due to local band bending, with a P+Q stress of 414 MPa. Below 3Sm (3x184=552 MPa) this passes the primary plus secondary stress limit.

> PF1b: Fig. 4.3.11-8 shows a very similar situation in the PF1b structure. The EM loads are also based on EQ10, but the WP finishes the pulse at a slightly warmer 100ºC. Primary plus secondary stress linearization at the max stress location shows a P+Q stress of 454 MPa, which is also acceptable (<552 MPa).

> PF1c: Fig. 4.3.11-9 shows the stress in the PF1c coil case. Like the PF1b result, the EM loads are based on EQ10 and the WP is at 100ºC. In this case, the max primary plus secondary stress linearization of 555 MPa occurs at ¼" radius of the coil case base. This is essentially right at the stress limit of 552 MPa.

Performing a cyclic evaluation requires tracking the total (often called "peak") stress history, which includes thermal stresses. This is presented in the following section.

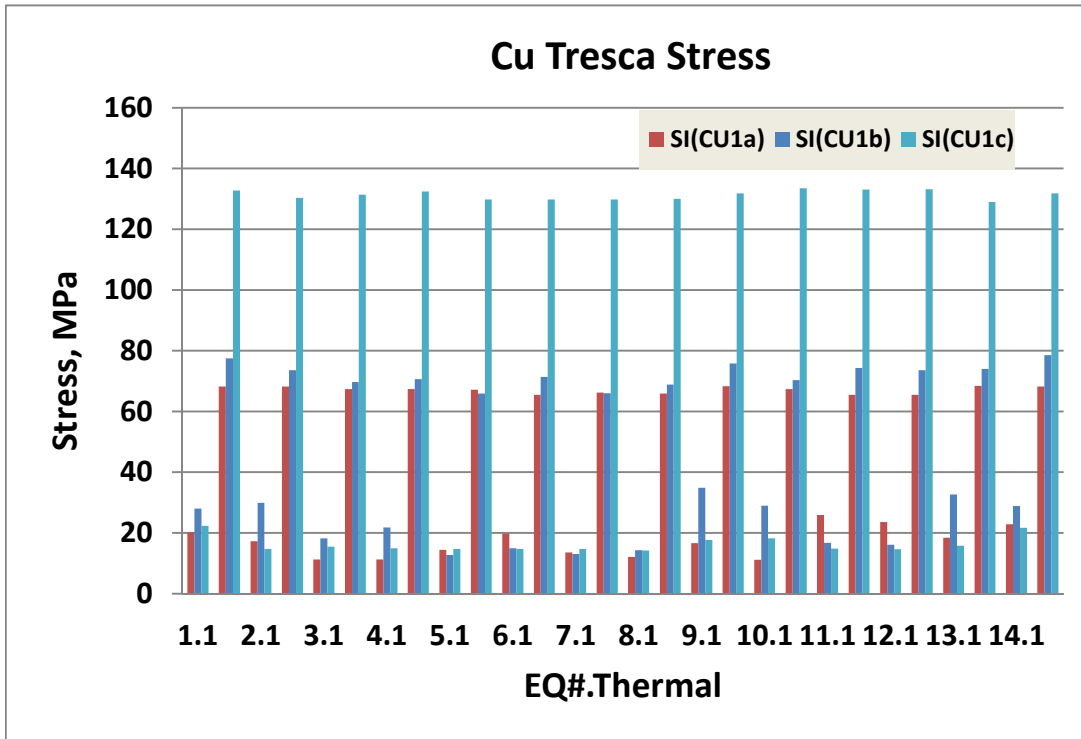Fig. 4.3.11-4 Tresca stress in PF1 Cu conductor (EQ1-EQ14, RT & Warm)

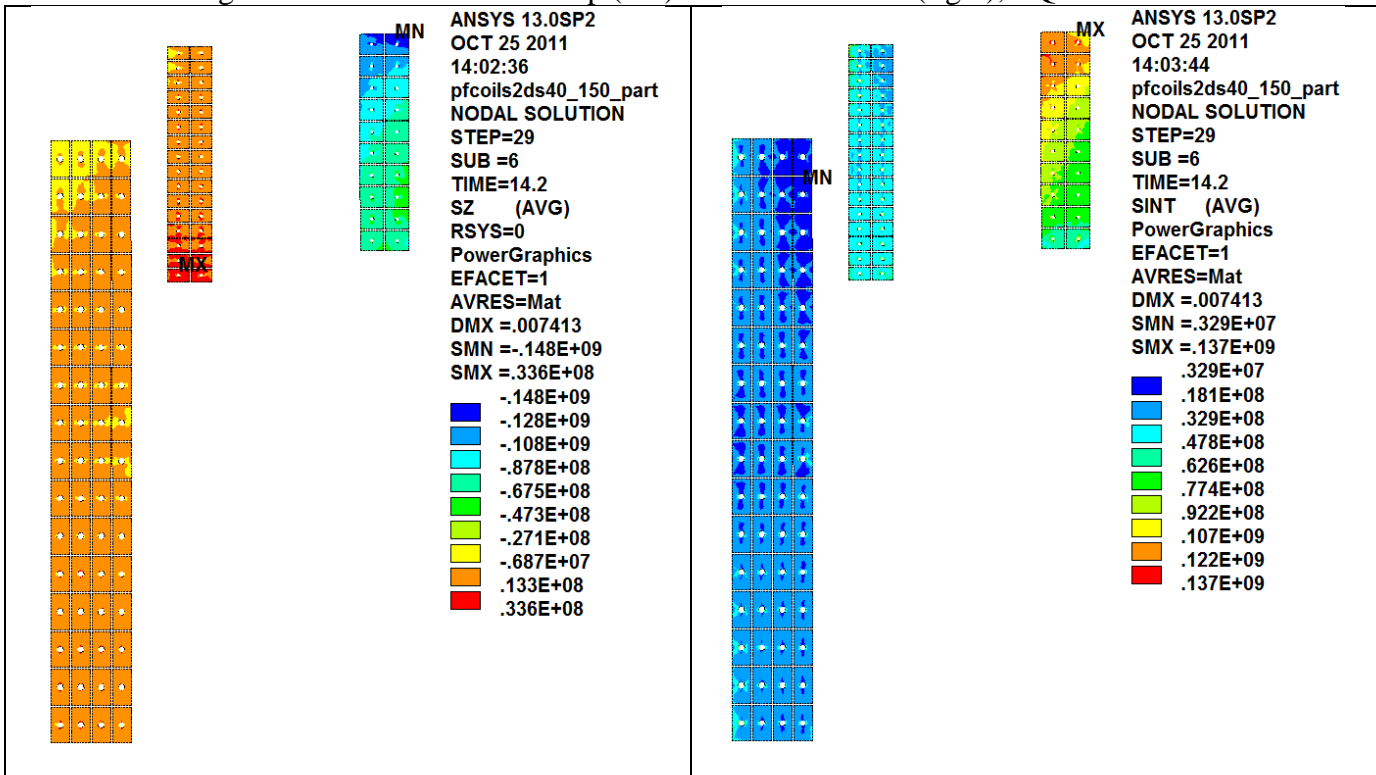Fig. 4.3.11-5 PF1a/b/c Cu Hoop (left) and Tresca Stress (right), EQ14 EM + Thermal

Fig. 4.3.11-6 Tresca stress in PF1 316SS Coil Cases (EQ1-EQ14)
(Stress values converted to ETAB values for sorting, which are generally less than Nodal results)
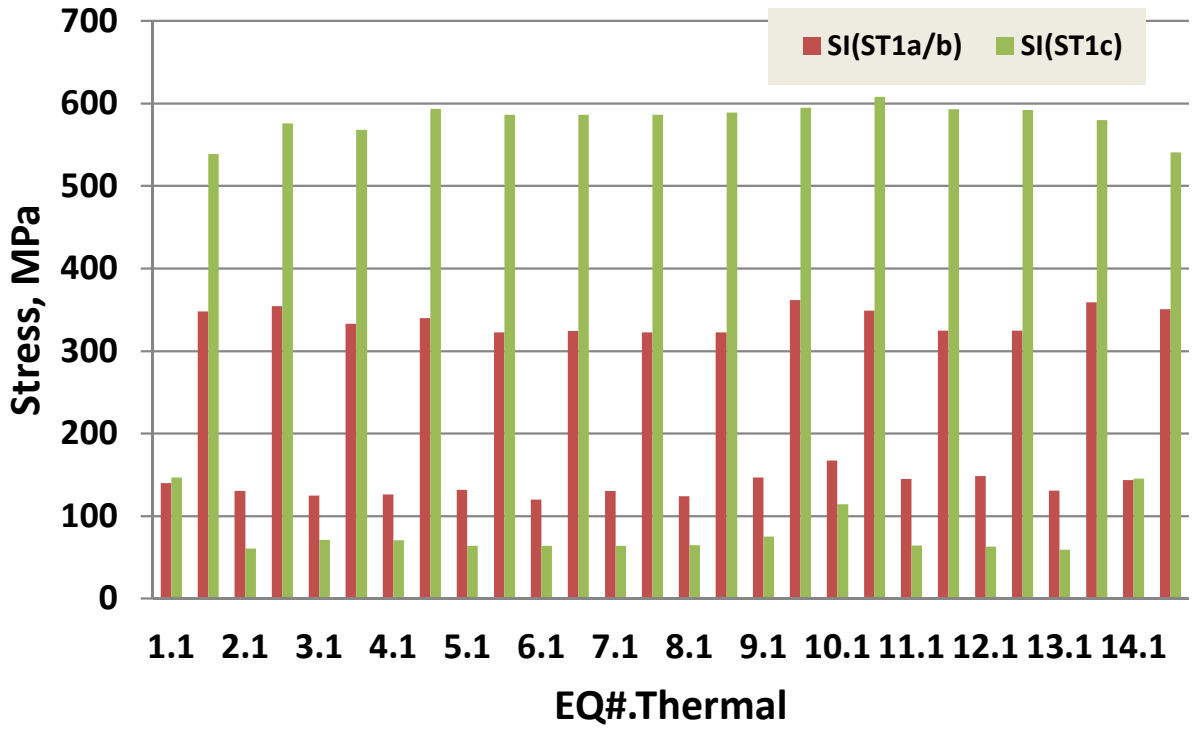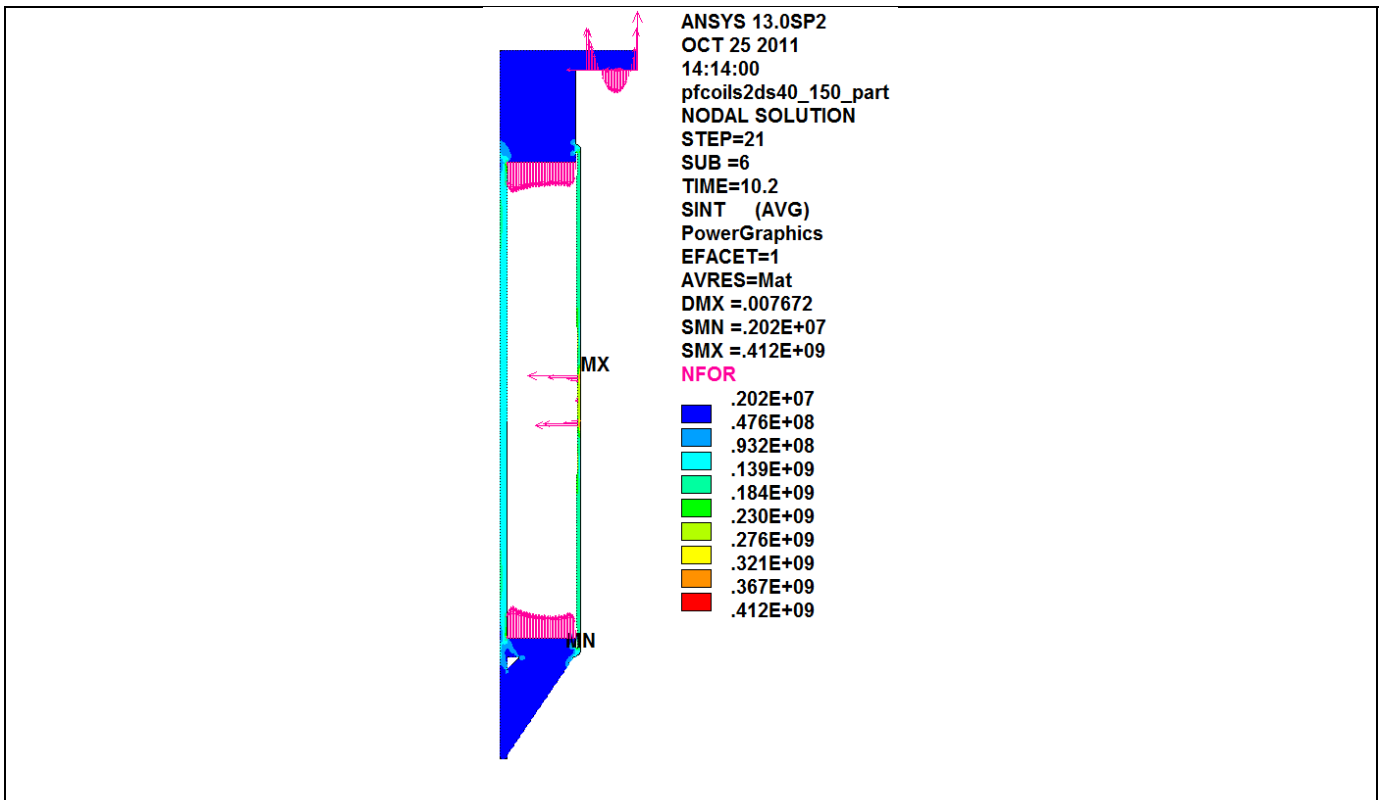
Structure Tresca Stress

Legend: ■ SI(ST1a/b) ■ SI(ST1c)

Y-axis: Stress, MPa (0 to 700)

X-axis: EQ#.Thermal (1.1, 2.1, 3.1, 4.1, 5.1, 6.1, 7.1, 8.1, 9.1, 10.1, 11.1, 12.1, 13.1, 14.1)

Fig. 4.3.11-7 Tresca stress and Linearization, PF1a structure (EQ10, WP at 85ºC)

Fig. 4.3.11-8 Tresca stress and Linearization, PF1b structure (EQ10, WP at 100ºC)

Fig. 4.3.11-9 Tresca stress and Linearization, PF1c structure (EQ10, WP at 100ºC)

4.3.12 Fatigue Analysis

The fatigue qualification of the Inner PF coil structures is based on the max (total, peak) stress levels shown in the stress plots shown in section 4.3.11 and the max coil temperatures and actual cycles (n_i) defined by Neumeyer's Pulse Spectrum spreadsheet (NSTX_CSU_Pulse_Spectrum.xlsx, 11 Dec 2011). Max coil case stresses are scaled proportional to the temperature rise divided by the analyzed temperature rise. An allowable number of cycles (N_i) is determined for each operating pulse based on this scaled stress level and the design-basis S-N fatigue curve (Fig. 4.1-2). The ratio of actual number of pulses divided by the allowable number of pulses for each "i" pulse yields the usage factor (U_i) for that stress cycle. The sum of all usage factors results in the cumulative usage factor (CUF_i), which must be less than unity to qualify the fatigue life of the structure. This is all done in an embellished version of Neumeyer's Pulse Spectrum spreadsheet (NSTX_CSU_Pulse_Spectrum CN0 LM1.xlsx). The net result is shown in Table 4.3.12-1 which indicates:

- Cyclic stresses in the PF1a structure are acceptable
- Cyclic stresses in the PF1b structure are too high, but only need to be reduced from 452 to <415 MPa
- Cyclic stresses in the PF1c structures are too high and need to be reduced from 756 to <488 MPa

While a reduction in PF1b structure stress level can be achieved with a slightly thicker OD band (see the following section), the more significant reduction in the PF1c structure stress level will require a more significant change.

Table 4.3.12-1 Preliminary S-N Fatigue Evaluation of the Inner PF Coil Structures

Inner PF Coils	Cyclic Stress at Max Coil Temp (MPa)	CUF=$\Sigma(n_i/N_i)$<1.0?	Cyclic Stress Limit to Achieve CUF<1 (MPa)
PF1a	412	0.06	575
PF1b	452	2.0	415
PF1c	756	35.7	488

4.3.12.1 PF1b Design Adjustment

The limiting stresses in the PF1b outer band shown in Fig. 4.3.11-8 are addressed here. Two parameters which influence this peak stress are band thickness and OD contact height. Fig. 4.3.12.1-1 shows how the stress can be minimized by varying the extent over which the coil engages the band. In addition, the plot includes two different band thicknesses. We see that the peak stress can be brought to 400 MPa for this critical loading condition with a 3/16" thick band and a contact height of 20%. The model is adjusted and the stress plot in Fig. 4.3.12.1-2 shows the acceptable result. This reduced peak stress is entered into the fatigue calculation spreadsheet and the revised CUF is 0.73 (<1.0✔).
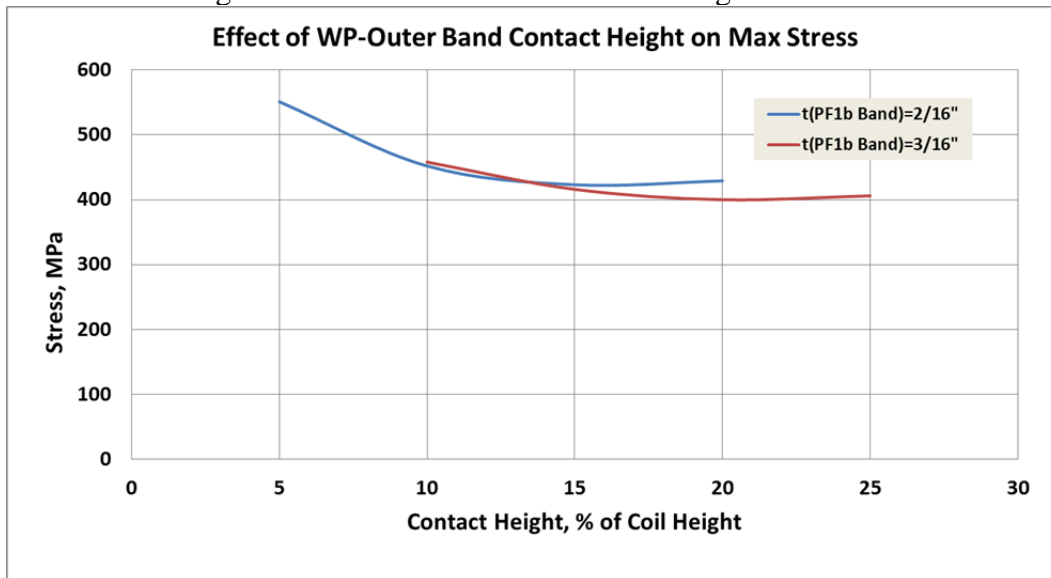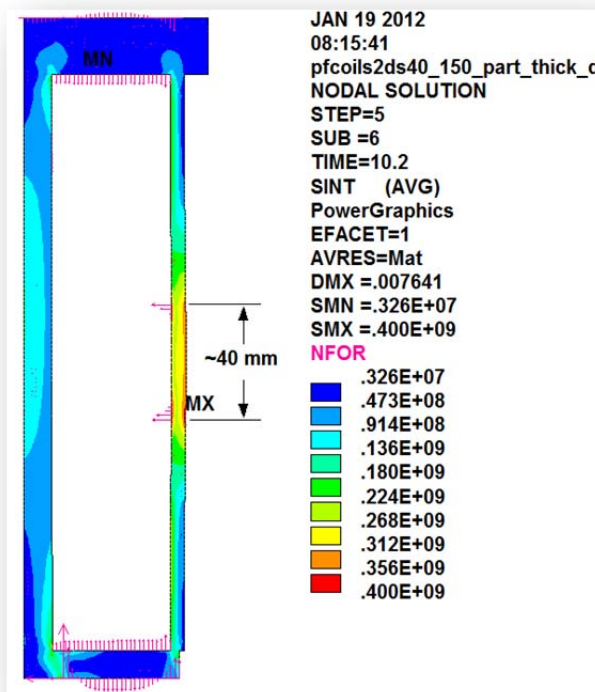
Fig. 4.3.12.1-1 Effect of OD Contact Height on Stress

Fig. 4.3.12.1-2 Optimized OD Contact Height (20% of Coil Height)

4.3.12.2 PF1c Design Adjustment

The limiting stresses in the PF1c outer band shown in Fig. 4.3.11-9 are addressed here. High stresses at the top and bottom of the outer case wall develop because of the coil's thermal expansion. This problem is solved in the PF1a and PF1b coils by using a relatively thin outer band and limiting coil/band contact to a small region around its mid-height. Fig. 4.3.12.2-1 shows how the stress can be reduced to an acceptable level (as defined in Table 4.3.12-1) by employing a 1/8" thick outer band and limiting the extent over which the coil engages the band to <20 mm. This reduced peak stress is entered into the fatigue calculation spreadsheet and the revised CUF is 0.92 (<1.0✔).

Fig. 4.3.12.2-1 Optimized OD Contact Height (10% of Coil Height)
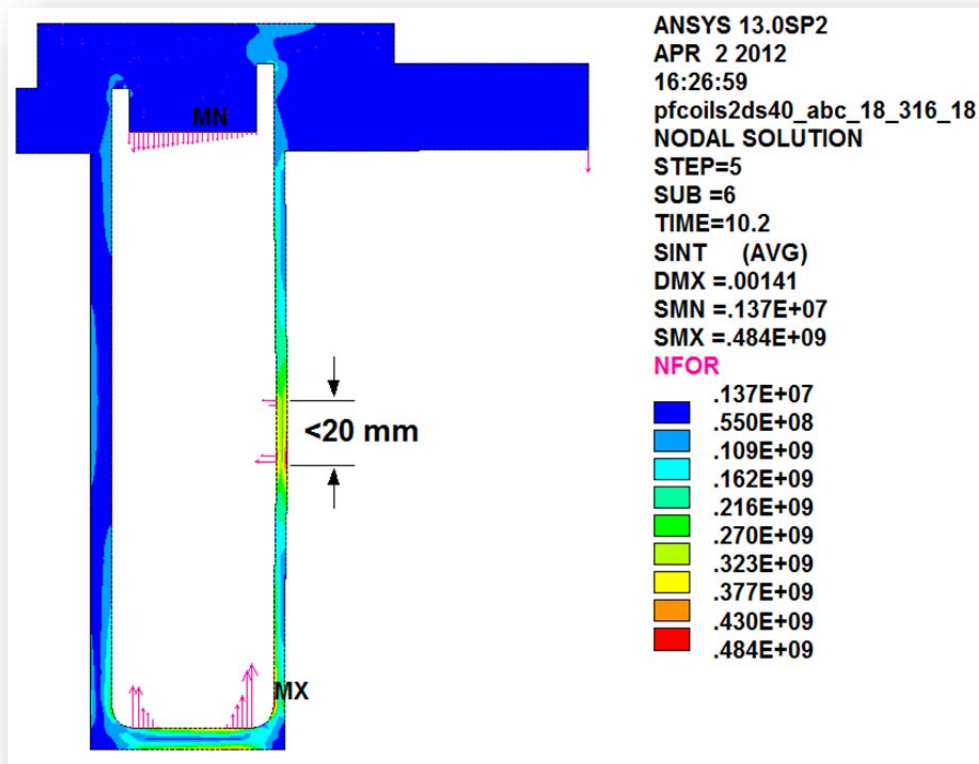
4.4 Stress Results: 3D Modeling

4.4.1 Worst-Case Stresses in PF1a/b Mandrel

The highest loading on PF1a structure is caused by EQ1 (TIME=14). As described for the 2D model:
- PF1aU pushes down (-96kip)
- PF1bU pushes up (83kip)

Rather than model the WP explicitly, the expected triangular shaped pressure profile (seen in the 2D model) is applied to the appropriate flanges. In the 2D model, the max stress of 140 MPa occurs in the PF1a winding shell, just below the heavy ring.
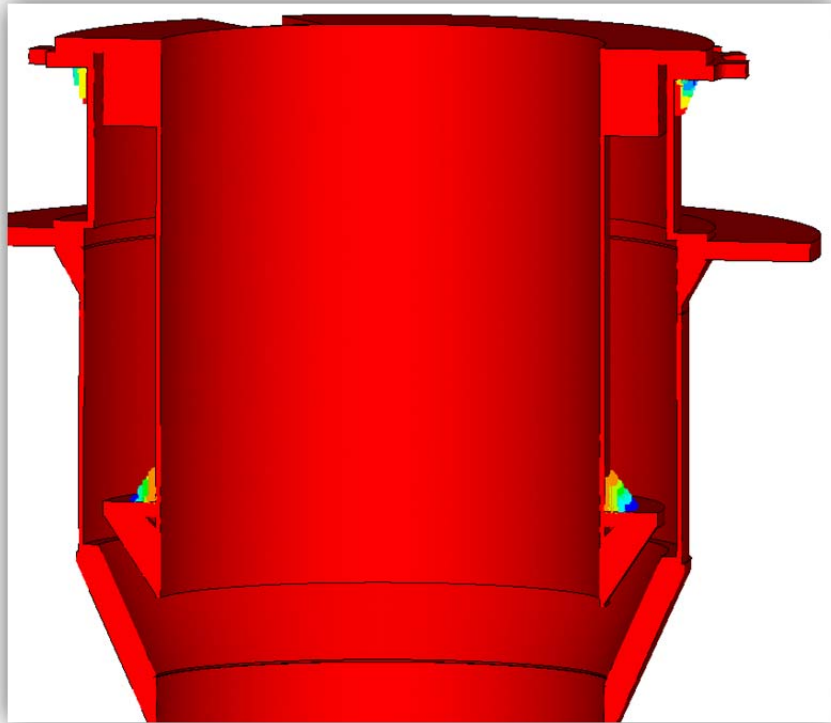

Fig. 4.4.1-1 Full 360º model sectioned to expose 3D features and equivalent pressure gradient loading

As shown in the left image of Fig. 4.4.1-2, the 3D PF1a/b model reproduces the max axisymmetric mandrel stress of 140 MPa away from the most significant 3D structural features. Gussets at the bottom flange fix the old roll-over problem of the earlier design.

The winding shell flexure at the lead opening produces some significant local stresses, with a localized peak stress of 300 MPa (FE singularity up to 520 MPa). Stress categorization is as follows:

- MEM=156 <184 MPa 👍
- M+B=340 MPa >276 MPa 👎
- Total Stress = 520 MPa >350 MPa 👎

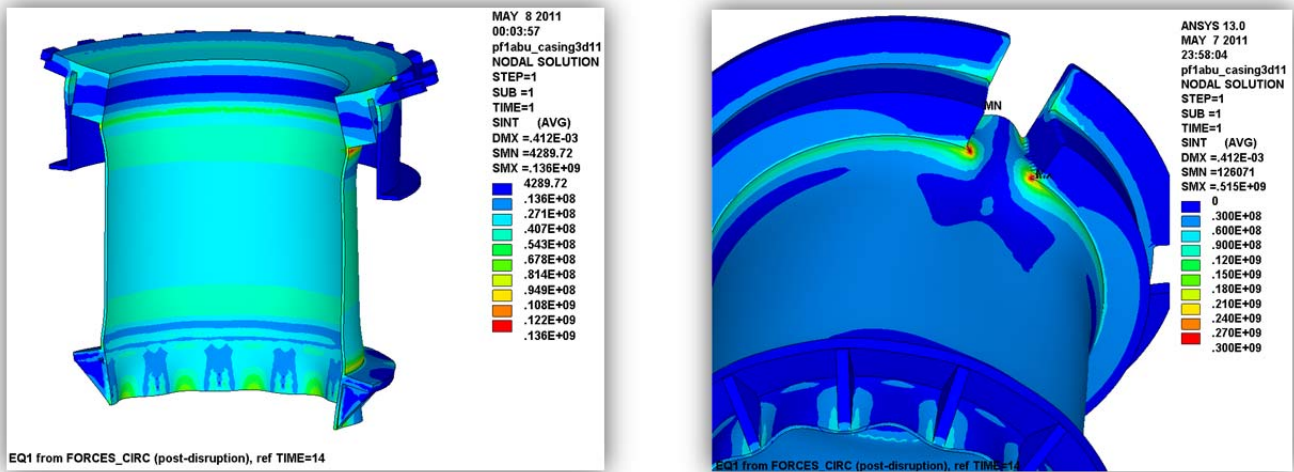Design requires a fix to reduce these high shell stresses in the region of the lead slot.

Fig. 4.4.1-2 Tresca Stress in PF1a/b Structure away from lead slot (left) and in region of lead slot (right)

High stresses in the PF1a lead slot and the potential for asymmetric radial movement during the warm end-of-pulse condition has led to the implementation of a 1/8" band-like cover structure for PF1a and 1b. This change to the structure, shown in Fig. 4.4.1-3, requires a structural re-evaluation since flange displacements and coil expansion will load the band and accompanying welds.
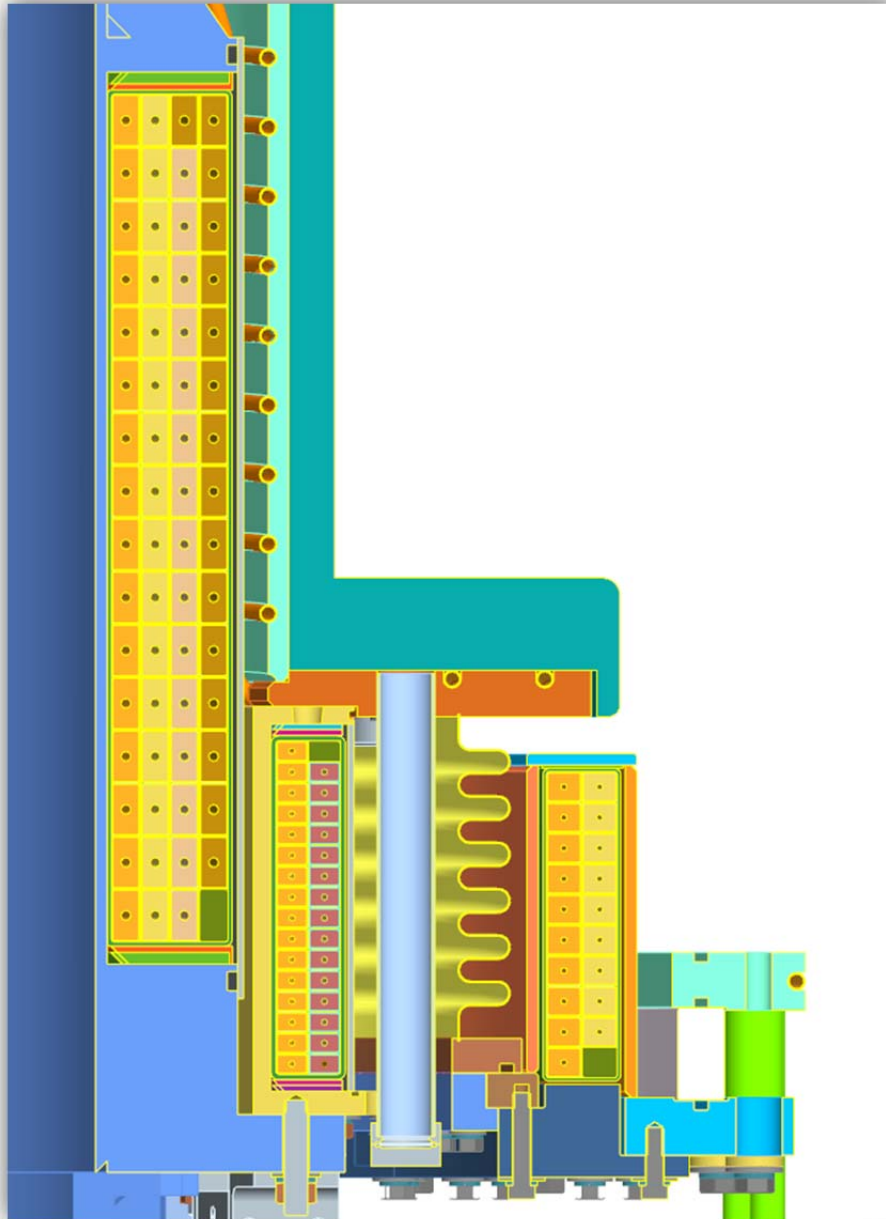

Fig. 4.4.1-3 Updated design showing addition of outer bands on PF1a and 1b coils

When a 1/8" outer band is added to the PF1a and PF1b mandrels, the local stress around the lead opening is decreased to level suitable for 316. Fig. 4.4.1-4 shows the worse-case Tresca stress in the revised PF1a and 1B structure and lists the stress categories required for static and fatigue evaluation.

- MEM: 93 MPa (<161 MPa)
- M+B: 207 MPa (<242 MPa)
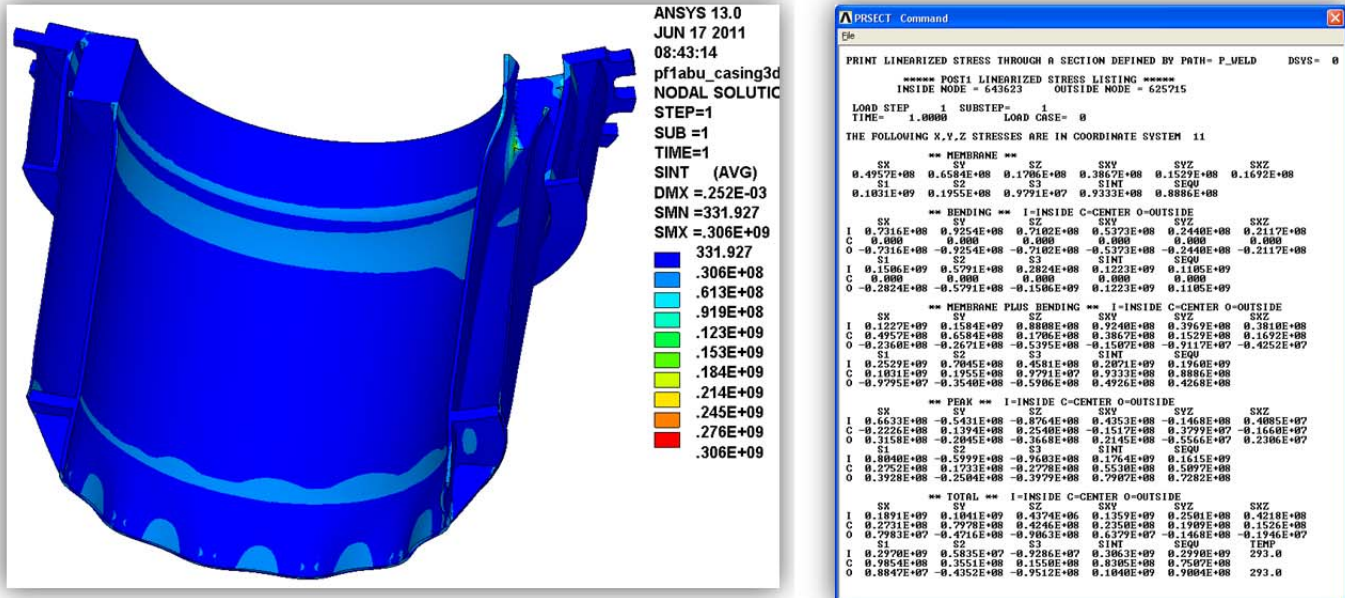- Total: 306 MPa (<350 MPa, cyclic stress limit)

Fig. 4.4.1-4 Tresca Stress in PF1a & 1b Reinforces Structure (left) and Stress Categorization (right)

The local stress in the 316SS PF1b is also improved by the external bands. Fig. 4.4.1-5 shows the worse-case Tresca stress in the revised 1B structure and lists the stress categories required for static and fatigue evaluation. Results indicate acceptable stress levels for a 316 SST structure.

- MEM: 45 MPa (<161 MPa)
- M+B: 86 MPa (<242 MPa)
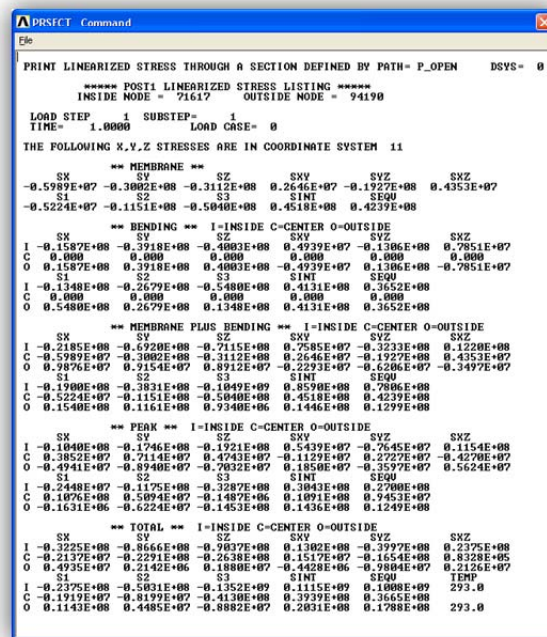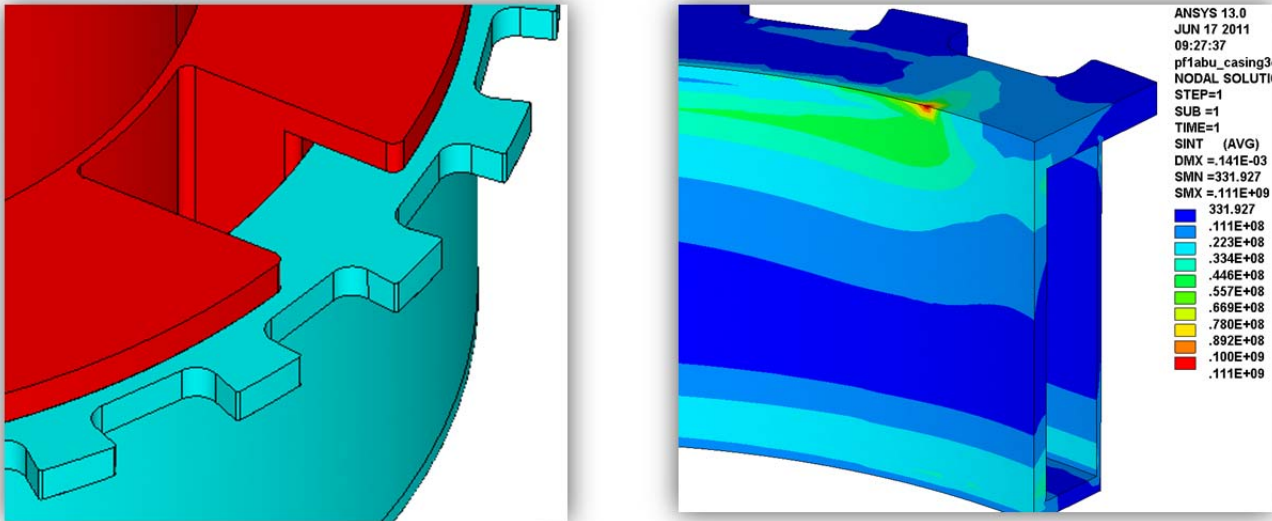- Total: 111 MPa (<350 MPa, cyclic stress limit)

Fig. 4.4.1-5 Close-up view (top-left), Tresca Stress (top-right) and Stress Categorization (bottom)

4.4.2 Worst-Case Stresses in Center Casing

The 2D model identifies EQ31 (PF_Currents_Forces) as producing the max vertical tensile stress in the structure, as PF1a/b upper and PF1a/b lower pull away from the mid-plane with 56 kip. In this top-half symmetry model, 12.7 and 43.3 kip are applied to the PF1a and PF1b upper flanges, respectively. Fig. 4.4.2-1 shows the Tresca stress in the center casing and PF1a/1b structure from this EQ31 loading. Notice that the max stress of 45 MPa appears in the center column to transition piece weld, which is comparable to the 50 MPa 2D result (<390 MPa static M+B limit and 375 MPa cyclic limit for INCONEL 625).
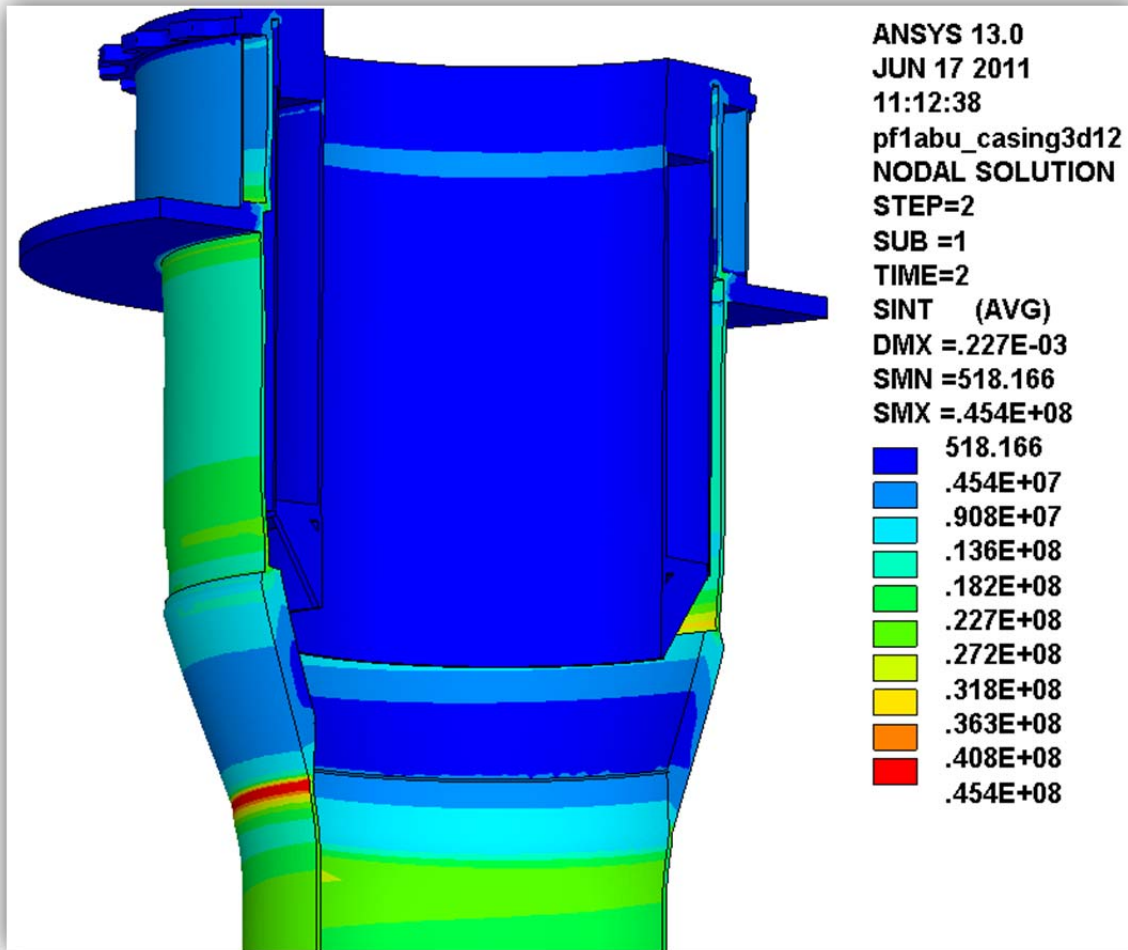

Fig. 4.4.2-1 Tresca stress in center casing and PF1a/1b structure from EQ31 Loading

4.4.3 Mechanical Performance of PF1c

The PF1c has 3D features which cannot be simulated with a 2D model. Here, the analysis focuses on the coil case, ceramic break and bolted flanges. Contact elements are used to model the interaction between the various parts. O-rings and their grooves are omitted for modeling simplicity. Bolts are modeled as 0.56" (matching the thru-hole diameter) instead of 0.5" as-designed. They are preloaded to an appropriate stress level. their and worst-case coil loads are applied: -32.6/+60 kip

Fig. 4.4.3-1 shows the model (including vessel sector) vertical deformation plots associated with:
STEP 1: Bolt Preload. Flange spacer height sized line-to-line with ceramic break, causing rotation.
STEP 2: -32.6 kip downward load reverses the flange rotation, flanges nearly parallel
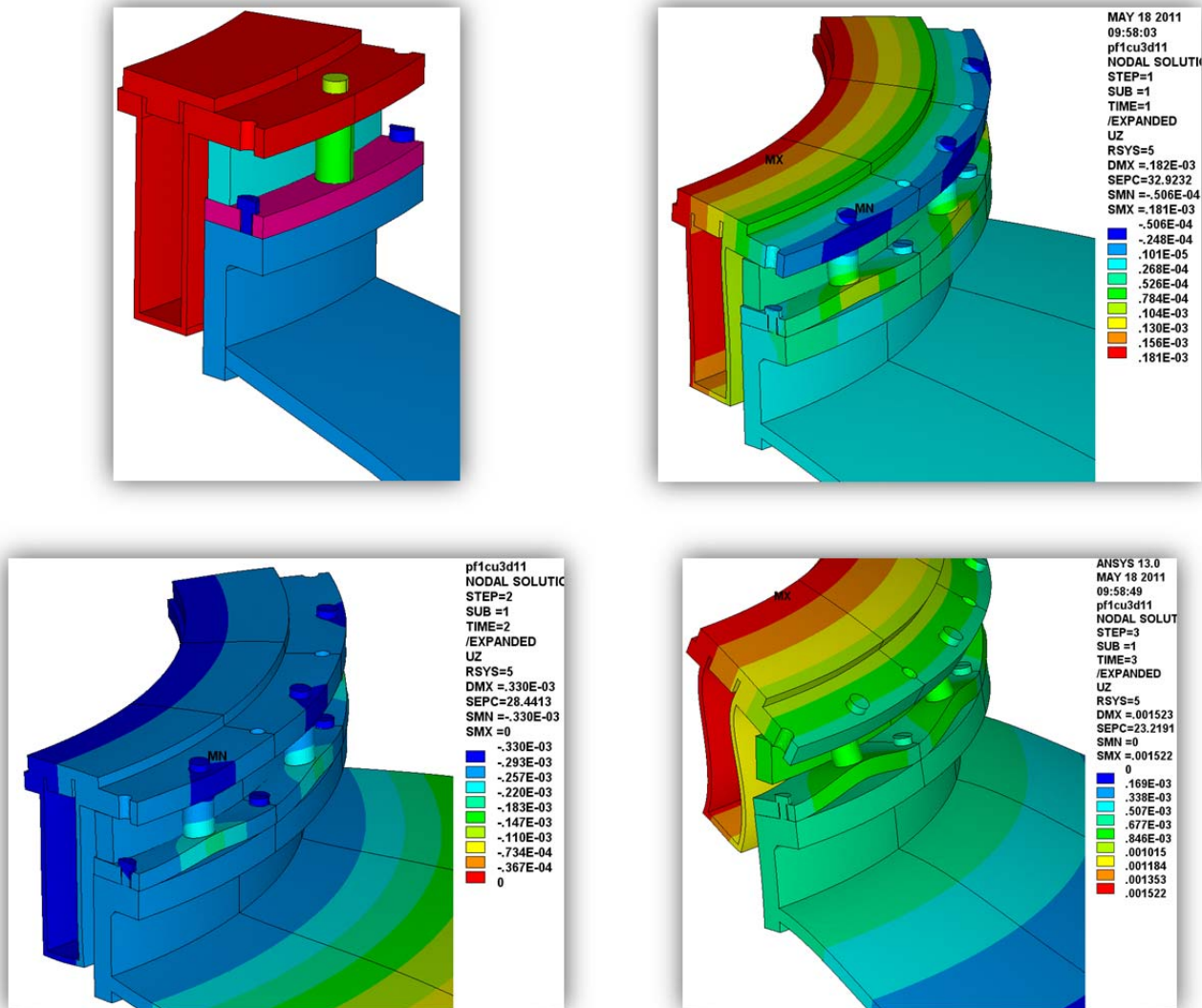STEP 3: +60 kip upward load exacerbates flange rotation

Fig. 4.4.3-1 3D Model of PF1cU (including vessel sector) and various vertical deformation plots

When the PF1cU coil experiences a large (60 kip) vertical load, flanges pry open at the ceramic break (AD-96 Alumina) and results in the following observations as seen in Fig. 4.4.3-2:

- 0.12 to 0.20 mm gap at the seal (5-8 mil)
- Bolt tensile stress range of ~100 MPa (max launch load case minus max centering load case, focusing on shank stresses)
- -200 MPa compressive stress (S3) in ceramic break from preload (bottom left)
    - matweb.com (CoorsTek AD-96 Alumina) compressive Strength: 2068 MPa
    - NSTX Structural Design Criteria: Sc<(2/3)SU = 1400 MPa
    - Semiconductor industry practice: Sc<(1/7)SU = 300 MPa
- Contact lost with 60 kip launching force (~zero stress in ceramic break with, bottom right).

Conclusion: Need to adjust stand-off height to limit interaction to O-ring compression (done by L. Morris).
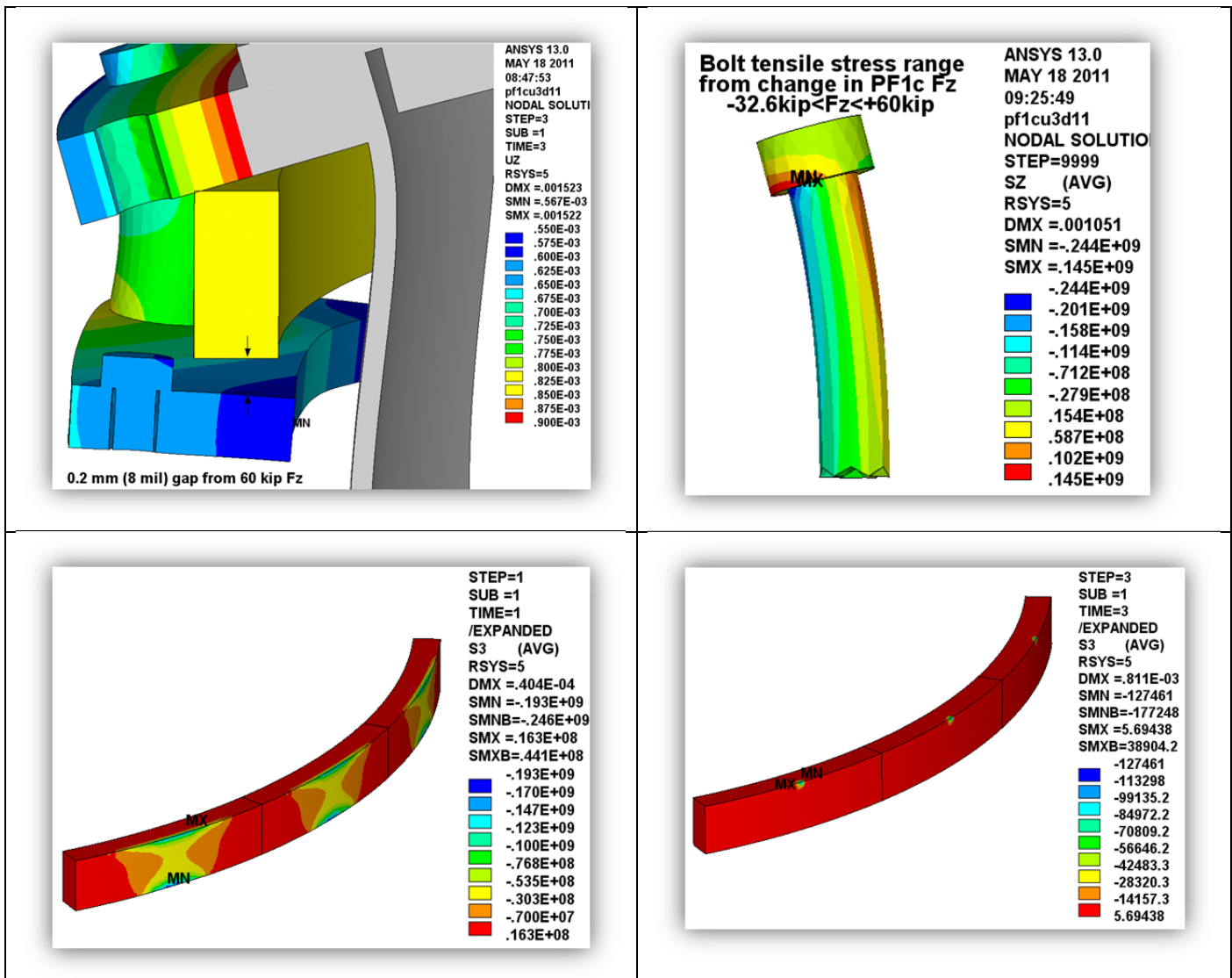

Fig. 4.4.3-2 UZ displacements (contours set to determine O-ring flange gap), Bolt Stress Range

The max coil PF1cU case stress occurs when the 60 kip launch load is applied. Fig. 4.4.3-3 shows the 3D model results and a max stress of 195 MPa, which is almost exactly the 2D result. A section through the outer shell indicates the limiting static MEM+BEND stress of 184 MPa, which is below the 242 MPa static stress limit for a 316 SST weld, and well below the 350 MPa max stress for S-N fatigue.
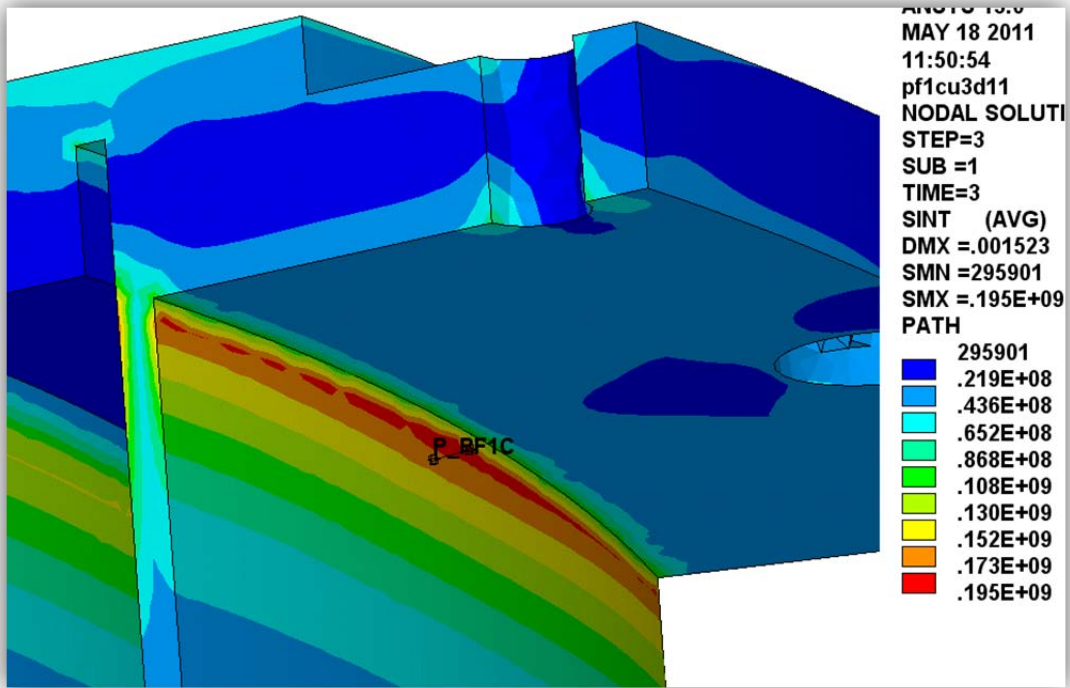
```
            ** MEMBRANE PLUS BENDING **   I=INSIDE C=CENTER O=OUTSIDE
      SX          SY          SZ          SXY         SYZ         SXZ
I -0.6752E+06 -0.8287E+08 -0.1836E+09 -0.2817E+06  0.6956E+06 -0.7544E+07
C -0.3227E+07 -0.2978E+08 -0.5249E+07 -0.6940E+05  0.3977E+06 -0.3905E+07
O -0.5779E+07  0.2331E+08  0.1731E+09  0.1429E+06  0.9979E+05 -0.2673E+06
      S1          S2          S3          SINT        SEQU
I -0.3635E+06 -0.8286E+08 -0.1839E+09  0.1835E+09  0.1592E+09
C -0.2011E+06 -0.8269E+07 -0.2978E+08  0.2958E+08  0.2649E+08
O  0.1731E+09  0.2331E+08 -0.5781E+07  0.1789E+09  0.1662E+09
```

Fig. 4.4.3-3 PF1c 3D model Stress contours and Linearized MEM+BEND Stress

4.5 Center Stack Casing Upper Support

Dynamic simulations of the Center Stack Casing's response to halo currents produced during a plasma disruption are presented in [5]. The lateral loads can reach ~250 kN which must be carried by the anchor bolts at the lower support, and across PF1cU into the vessel. In the present design, these loads must go through the relatively soft bellows. However, recent activities focus on providing a stiffened load path between the center stack and vacuum vessel through a bumper-type support connecting the PF1b/PF1c mandrels. The analysis presented here is used to determine the stiffness of the various elements of the load path which serves as input to a revised dynamic simulation.

Fig. 4.5-1 shows a plot of the 180° model of PF1cU, the ceramic break hardware (minus the ceramic ring) and the vacuum vessel head. A lateral load of 126 kN is applied to a patch of nodes on the inside flange of the PF1cU coil case. The deformed shape plot shows flange rotation, stand-off hardware deformations and a local displacement of 2.14 mm. A 210 MPa bolt preload and flange face friction coefficient of 0.3 are sufficient to prevent sliding from this static load application. Accounting for the half-symmetry, the resulting overall stiffness is given by:

> $k_{(PF1cU+VV)} = F_{tot}/\delta x = 2(126kN)/(2.14 \text{ mm}) = 118$ kN/mm (670 kip/in)

Fig. 4.5-2 shows a plot of the model which represents the load path between the center stack casing and the PF1b OD flange bumper. In this case, the load direction is in negative X and the stiffness is determined by the differential displacement between the casing top flange and the bumper:
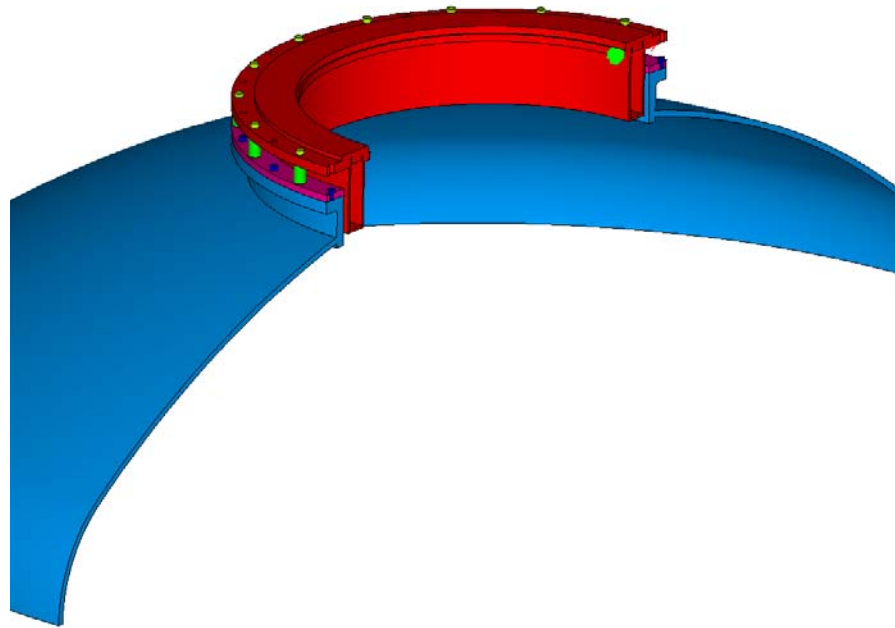
> $k_{(PF1bU+Casing Flng)} = F_{tot}/\delta x = 2(126kN)/(7.34\text{-}5.79 \text{ mm}) = 162$ kN/mm (930 kip/in)

The bellows is also in the load path between the casing top flange and the PF1c casing flange ID, although substantially softer [6]. These springs add parallel with an effective stiffness of (204+930) or 1130 kip/in. However, this spring constant is in series with the $k_{(PF1cU+VV)}$ calculated above. These springs are in series, which results in an effective stiffness of $(1/670+1/1130)^{-1}$ or 420 kip/in between the center casing top flange and the vacuum vessel through a single, zero-radial gap bumper.

Contact between the two coils at a single bumper is an extreme case and represents a (4) bumper configuration with the load direction such that only one bumper is engaged. If more bumpers are incorporated into the design, then the overall stiffness will be a higher, and the load will be carried by more structure. In this conservative calculation, the results from the applied 252 kN load are scaled by 0.441 to determine the stresses due to a 25 kip load through this upper support load path. Fig. 4.5-3 shows a plot of the PF1c coil case stress. Ignoring the contact stress identified by a single red spot, the general stress field is <300 MP. Linearization shows a MEM+BEND stress of ~200 MPa (<1.5Sm or 276 MPa). However, the lateral load could reach ~200 kN (45 kip). With a scale factor applied to the 252 kN load case of 0.794 (not 0.441), the MEM+BEND stress would be ~200 x (45 kip/25 kip) or 360 MPa. At this stress level, the number of bumpers must increase from four to at least six. Eight bumpers (one every 45°) is a reasonable distribution and leads to a more robust design.

Conclusion: A series of (8) bumpers should be located between the PF1bU mandrel top flange OD and the PF1cU case flange ID. This will result in a center casing upper support stiffness to ground of >420 kip/in. Brooks' dynamic simulation of halo currents and forces should adopt this effective stiffness value.

Fig. 4.5-1 PF1cU & Vessel Model, Lateral Displacement from 252/2 kN Bumper Load

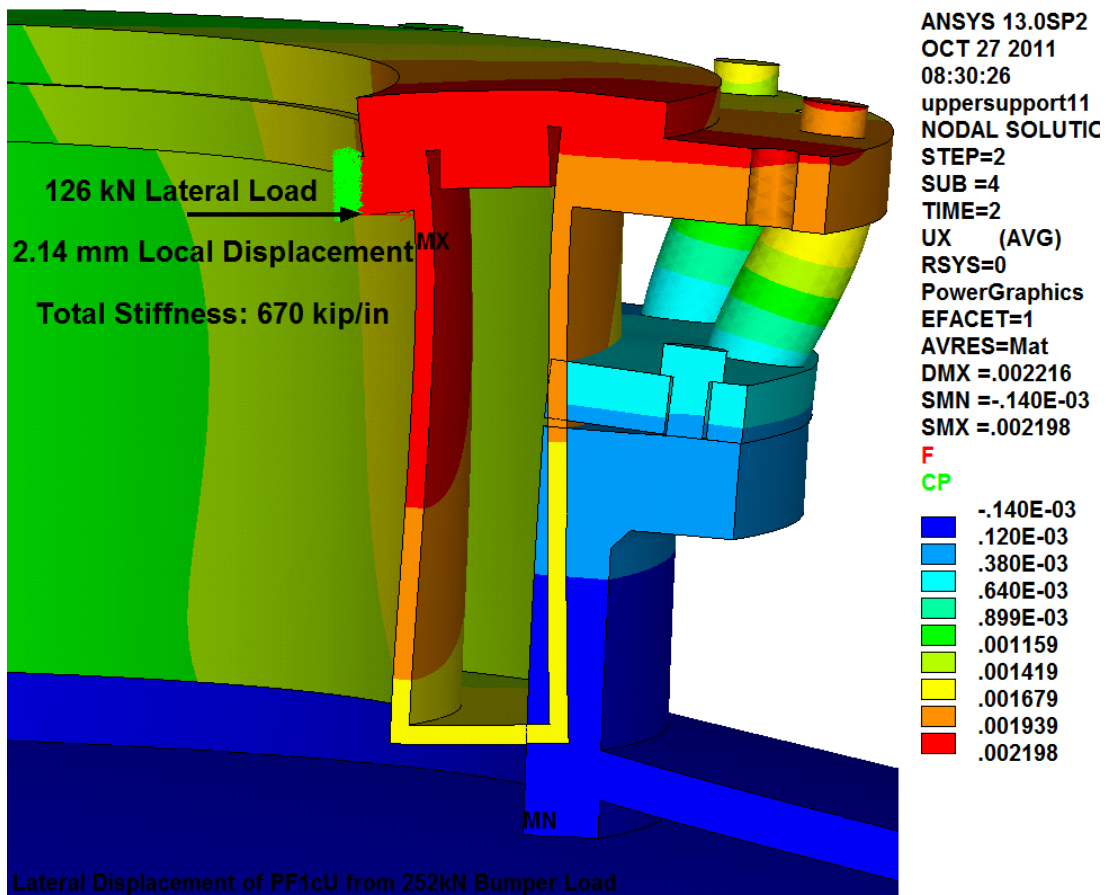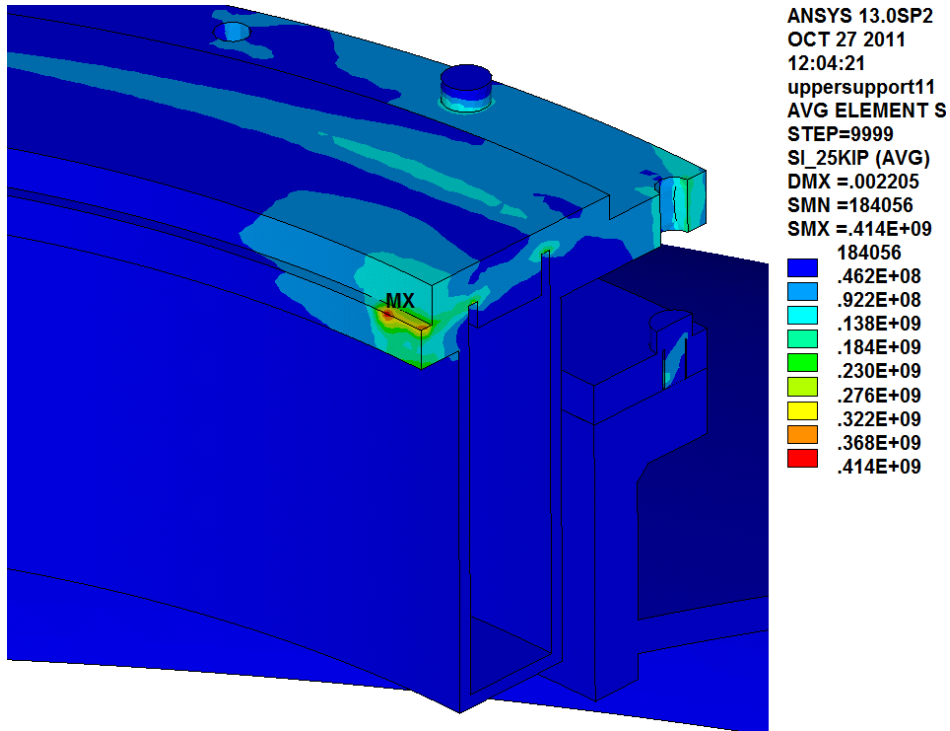Half-Model of PF1cU and Vacuum Vessel Head

126 kN Lateral Load

2.14 mm Local Displacement

Total Stiffness: 670 kip/in

ANSYS 13.0SP2
OCT 27 2011
08:30:26
uppersupport11
NODAL SOLUTIC
STEP=2
SUB =4
TIME=2
UX   (AVG)
RSYS=0
PowerGraphics
EFACET=1
AVRES=Mat
DMX =.002216
SMN =-.140E-03
SMX =.002198
F
CP

-.140E-03
.120E-03
.380E-03
.640E-03
.899E-03
.001159
.001419
.001679
.001939
.002198

Lateral Displacement of PF1cU from 252kN Bumper Load

Fig. 4.5-2 PF1a/bU & Center Casing, Lateral Displacement from -252/2 kN Bumper Load
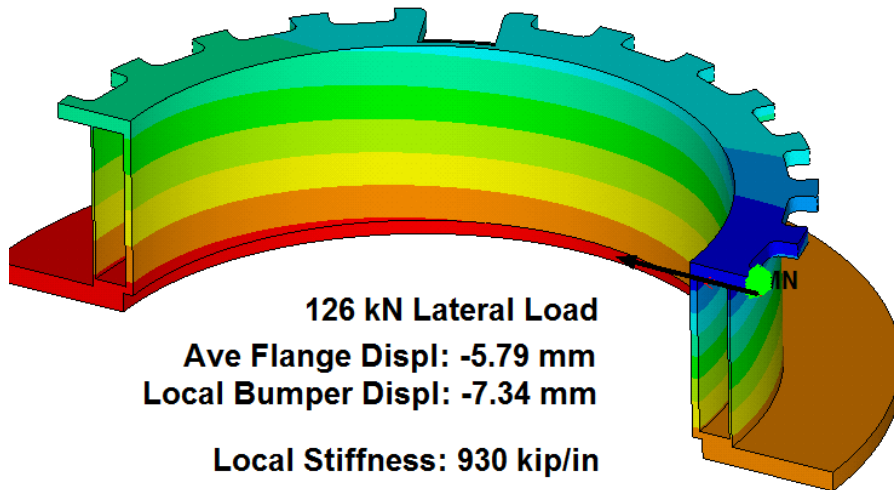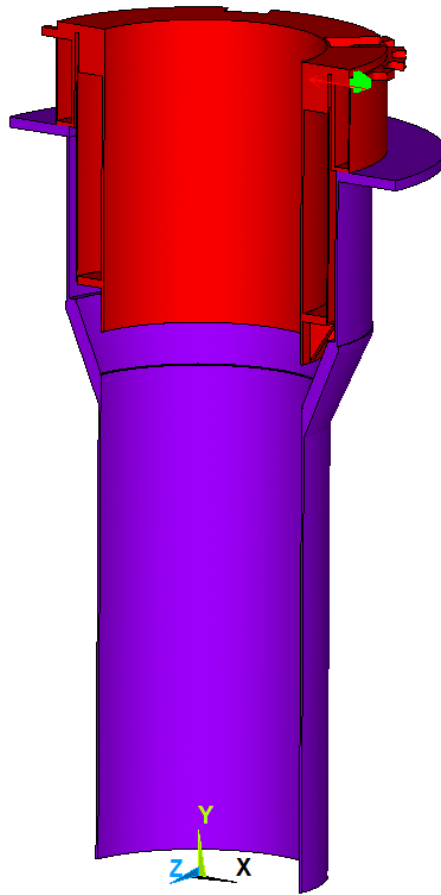
126 kN Lateral Load

Ave Flange Displ: -5.79 mm
Local Bumper Displ: -7.34 mm

Local Stiffness: 930 kip/in

uppersupport12
NODAL SOLUTIO
STEP=1
SUB =1
TIME=1
UX
RSYS=0
DMX =.007557
SMN =-.007336
SMX =-.00563
F
CP

-.007336
-.007147
-.006957
-.006767
-.006578
-.006388
-.006199
-.006009
-.00582
-.00563

Fig. 4.5-3 PF1cU Case Stress & Linearization, Single Bumper Contact Point (Stress from 25 kip load)

4.6 Terminal Support

The terminal supports for the PF1A and PF1B have been designed with tower brackets to hold the leads and counter the forces on the leads from the busbar, and from thermal gowth. Figure 4.6-1 shows the design of PF1A and PF1B coil terminal leads.
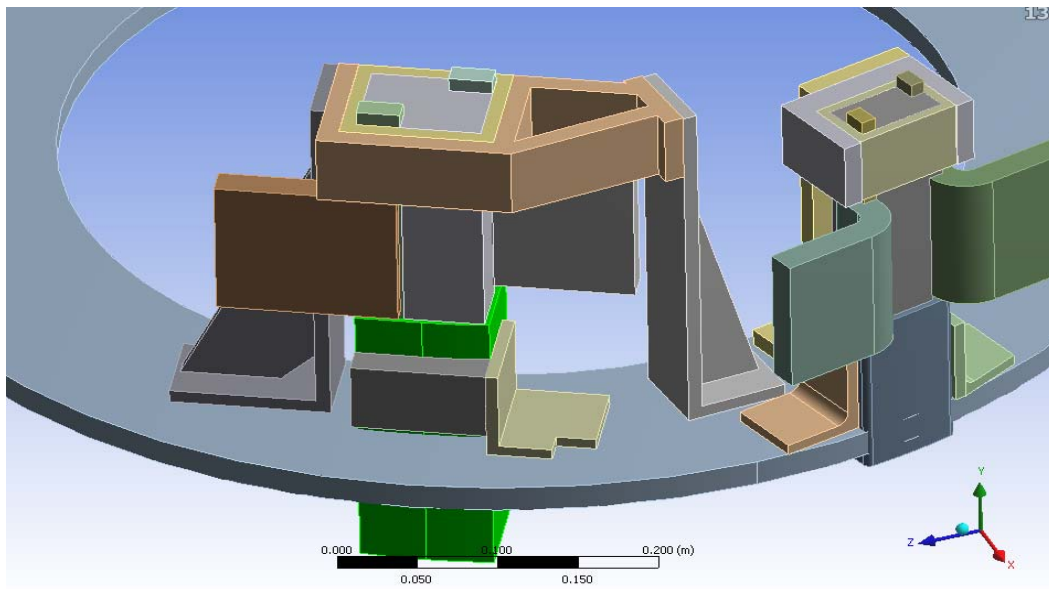

Figure 4.6-1

The PF coils leads move radially outward by 0.5 mm due to thermal growth of the coils. To allow this movement outward, we suggested that the angle brackets on the two sides of the lead stems be untied from the stem to allow the stem to move in the radial direction while the angle brackets are brought in to touch the stem and disallow toroidal displacement. To predict the stress on the coil leads we need to impose the radial displacement on the bottom of the lead stem as well as the forces and moments imposed from the busbars on the lead flags. Forces from the busbars to the lead input and output flags were calculated in the busbar analysis calculation (NSTXU-CALC-55-01-00). These forces are shown in table 4.6.1 and Figure 4.6-2.

	Forces on the flags					
	FX	FY	FZ	MX	MY	MZ
	N	N	N	Nm	Nm	Nm
P1AUI	-2.05E+03	1.29E+03	-5.84E+03	-1.83E+03	-1.89E+03	2.38E+02
P1AUO	-2.83E+03	1.02E+03	6.14E+03	-1.99E+03	-7.90E+03	3.55E+02
P1BUI	-1.56E+03	-7.33E+02	-6.02E+03	3.75E+02	-3.82E+02	-5.65E+01
P1BUO	1.64E+02	1.27E+03	6.85E+03	-4.06E+02	-2.18E+03	5.17E+02
P1CUI	-2.55E+02	8.66E+02	-1.49E+03	-9.31E+02	-1.39E+02	1.24E+02
P1CUO	-1.95E+03	1.30E+03	-9.61E+02	-2.08E+03	-3.50E+03	-4.27E+02

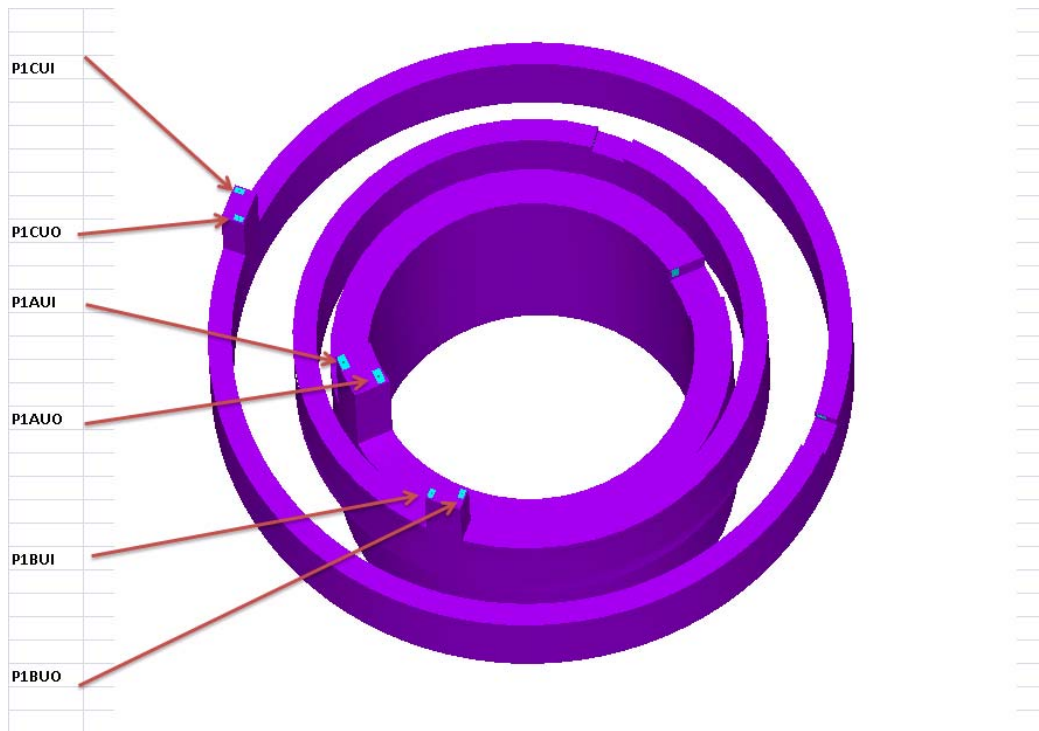Table 4.6-1 Forces on the lead IO flags for PF1A,B, and C coils.

Figure 4.6-2 Forces on the lead IO flags for PF1A,B, and C coils.

The resulting stress from applying the forces, moments and the displacement on the PF1Aand PF1B leads are shown in figure 4.6-3 and 4.6-4 respectively.
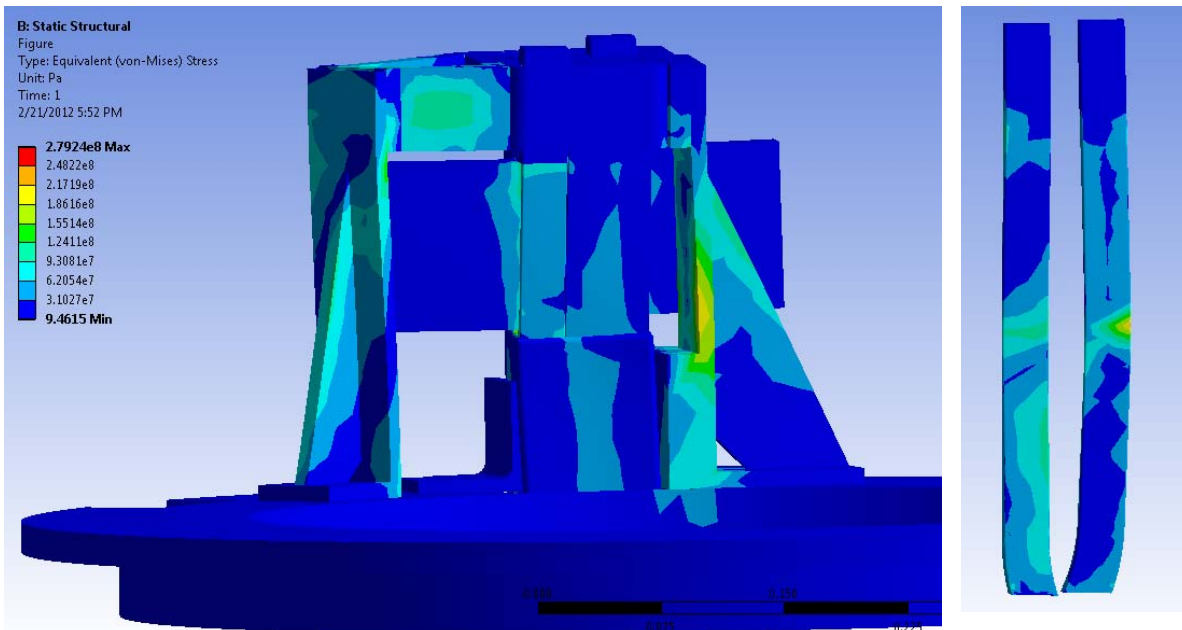

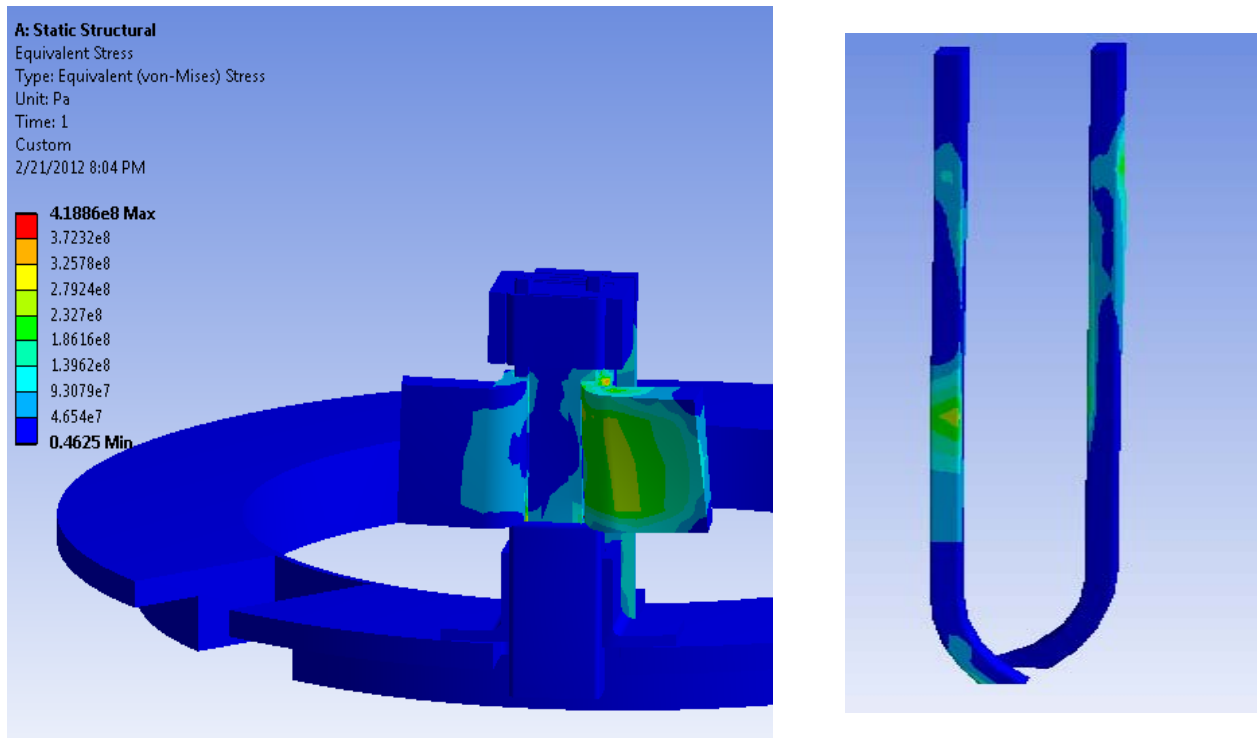Figure 4.6-3, Equivalent stress in the PF1A leads and conductors

Figure 4.6-4, Equivalent stress in the PF1B leads and conductors

As can be seen the stresses are too high for copper which has a fatigue allowable of 125 MPa. As stated by Andrei Khodak in the Busbar Calculation NSTXU-CALC-55-01-00, the internal PF busbar needs to be designed to exert lower forces and moments on the PF coil leads. They need to be designed to be a factor of 2.5 lower than the current ones in order for the copper and steel stresses to be acceptable.

4.7 Operating Limitations

Neumeyer's DPS contains a table summarizing the max & min radial and vertical coil forces with and without plasmas (Table 4.2.2-1). The table also lists "Worst Case Min" and "Worst Case Max" values. The latter load values can occur when the coils are driven to their power supply current limits, as opposed to a valid plasma equilibrium operating point (EQ). The ratios of the Worst Case loads to the valid EQ loads are presented graphically in Fig. 4.6-1 for radial (top) and vertical (bottom) load directions.

If allowed to operate at their power supply limits, PF1b could experience radially inward forces 47 times larger than the worst of the valid equilibria conditions. Conversely, PF1c could experience radially outward forces 16 times larger than the worst of the valid equilibria conditions. Vertical loads produced by coils operating at their power supply limit are not quite as dramatic (but still significant), with load ratios of two to seven times the valid equilibrium condition.

There is insufficient margin in the coil and support structure design to tolerate such large forces from coil currents at power supply limits. Consequently, some digital coil protection (DCP) algorithm must be designed to disallow much of this random coil operating space.

The DCPS calculates coil loads from the currents being requested by the operators, plasma position control system, and other operating parameters. A look-up function allows the DCPS to determine the radial and vertical loads and moments about the coil centroid at any instant in time. We will need to add some algorithm that relates the stresses of concern to these loads and moments. The DCPS will also be able to integrate the resistive losses ($\rho J^2 t$) to determine the temperatures of the coils at any instant. Since elevated coil temperatures lead to loads on the inner PF coil outer shells, some temperature limitations must be included in the stress algorithm.
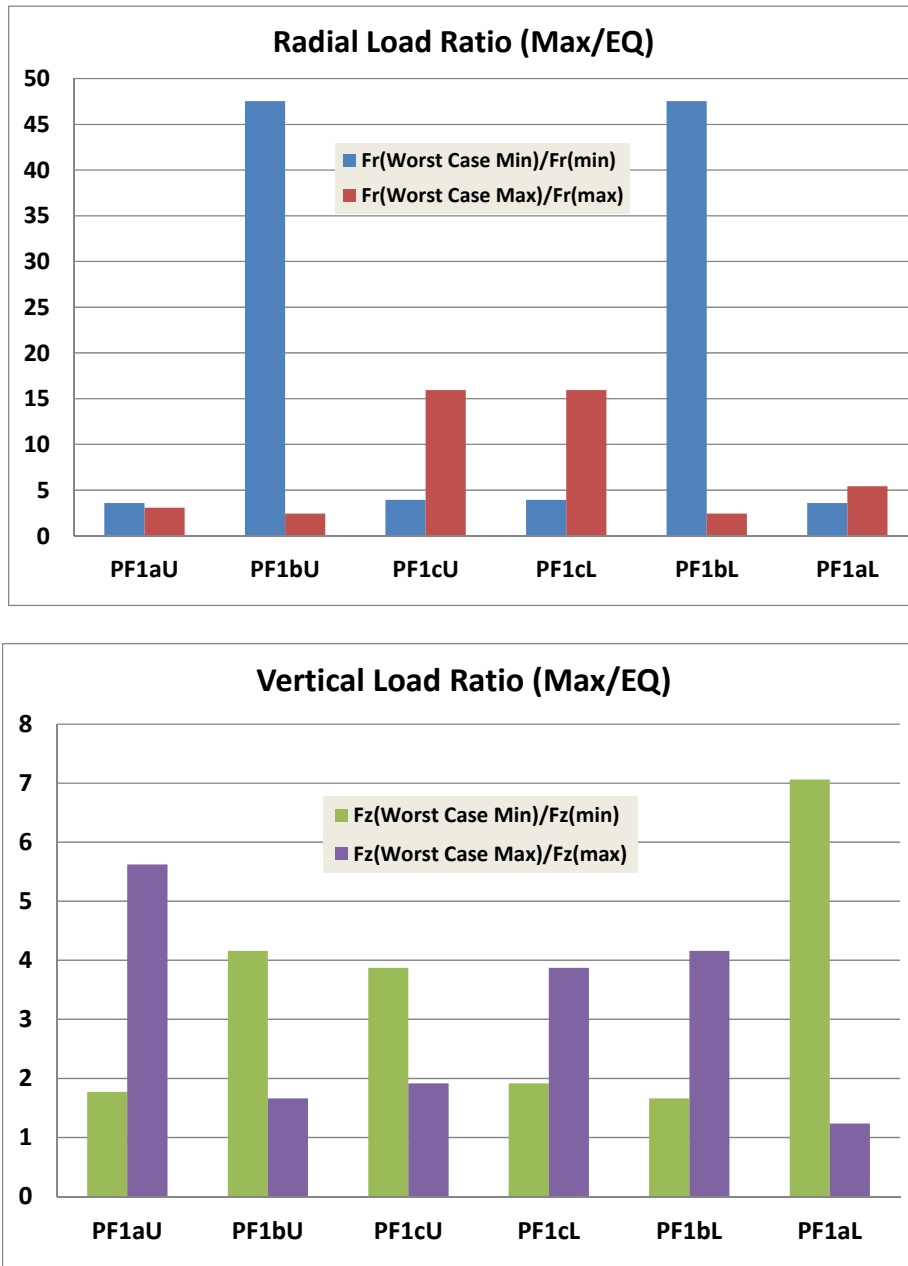

Fig 4.7-1 Max Radial & Vertical Coil Forces

5.0 Conclusions

A collection of electromagnetic and structural analyses of the inner PF coils is presented. The sheer number of potential plasma equilibrium and post plasma-quench operating points requires implementing an efficient scoping study and some screening rules in order to streamline the task. After all of this analysis, review and inspection, only a handful of operating points produce the most demanding conditions for these PF1 coils and their support structure. A few design changes are incorporated and add robustness to the structure. In particular, the addition of (8) bumpers equally spaced around the annular gap between the PF1bU mandrel and PF1cU top flanges help transmit lateral loads produced by Halo currents (ref. 5).

Copper and insulation stresses are well within design limits. However, the potential for much higher magnet forces is present if the coils operate at random currents anywhere close to the power supply limits. Therefore a DCP algorithm must be designed and implemented to ensure safe PF coil operation.

6.0 References

[1] C. Neumeyer, Design Point Spreadsheet, NSTX_CS_Upgrade_110317.xls

[2] I. Zatz, NSTX Structural Design Criteria, NSTX-CRIT-0001-01, Feb 2010

[3] P. Titus, OH Conductor Fatigue Analysis, NSTXU-Calc-133-09, Nov 2010

[4] CTD, Inc., "Fabrication and Testing of Cyanate Ester-Epoxy/Glass Fiber/Copper Laminates," PPPL PO PE010925-W, Oct. 7, 2011

[5] A. Brooks, Halo Current Analysis of Center Stack, NSTX-Calc-133-05-00, September 2011

[6] P. Rogoff, Center Stack Casing Bellows, NSTX-Calc-133-10-00, January 2011

7.0 Appendix

7.1 Mechanical properties of CTD-422 (P. Fabian e-mail to L. Myatt, 10/19/2011)

From: Paul Fabian [mailto:paul.fabian@ctd-materials.com]
Sent: Wednesday, October 19, 2011 11:25 AM
To: leonard.myatt@gmail.com
Subject: CTD Data at elevated temps

Leonard,

Unfortunately, we do not have any good modulus data on the CTD-425 resin system. However, we do have some through thickness compression data on CTD-422, which is a very similar resin system to CTD-425. Here's how the compression data for CTD-422 stacks up at RT and 373K:

At 295 K
Average compression strength = 890 MPa
Average compression modulus = 10.8 GPa

At 373 K
Average compression strength = 700 MPa
Average compression modulus = 10.9 GPa

The data above is for a S2 glass reinforced composite with a nominal 50% fiber volume fraction.

I hope this helps you out. Let me know if you need anything else.

Best regards,
Paul

Paul E. Fabian
Sr. Program Manager
Advanced Product Development, Manufacturing, and Testing
Composite Technology Development, Inc.
2600 Campus Drive, Suite D
Lafayette, CO 80026
Phone: 303-664-0394 x103
Fax: 303-664-0392